https://doi.org/10.5194/egusphere-2024-278
Preprint. Discussion started: 13 May 2024
© Author(s) 2024. CC BY 4.0 License.

Introducing the MESMER-M-TPv0.1.0 module: Spatially Explicit Earth System Model Emulation for Monthly Precipitation and Temperature

Sarah Schöngart[1,2], Lukas Gudmundsson[3], Mathias Hauser[3], Peter Pfleiderer[2], Quentin Lejeune[2], Shruti Nath[2], Sonia Isabelle Seneviratne[3], and Carl-Friedrich Schleussner[1,2]

[1]IRIThesys, HU Berlin, Friedrichstrase 191, 10117 Berlin, Germany
[2]Climate Analytics, Ritterstrasse 3, 10969 Berlin, Berlin
[3]Institute for Atmospheric and Climate Science, ETH Zürich, Universitätsstrasse 16, 8006 Zürich, Switzerland

Correspondence: Sarah Schöngart, sarah.schoengart@climateanalytics.org

Abstract. Emulators of Earth System Models (ESMs) are statistical models that approximate selected outputs of ESMs. Owing to their runtime-efficiency, emulators are especially useful whenever vast amounts of data are required, for example, for thoroughly exploring the emission space, for investigating high-impact low-probability events, or for estimating uncertainties and variability. This paper introduces an emulation framework that allows to emulate spatially explicit monthly mean precipitation fields using spatially explicit monthly mean temperature fields as forcing. The emulator is designed as an additional module within the MESMER(-M) emulation framework and its core relies on the concepts of Generalised Linear Models (GLMs). Precipitation at each (land-)grid point and for each month is approximated as a multiplicative model with two factors. The first factor entails the temperature-driven precipitation response and is assumed to follow a Gamma distribution with a logarithmic link function. The second factor is the residual variability of the precipitation field. The residual variability is assumed to be independent of temperature, but may still possess spatial precipitation correlations. Therefore, the monthly residual field is decomposed into independent Principal Components and subsequently approximated and sampled using a Kernel Density Estimation with a Gaussian kernel. The emulation framework is tested and validated using 24 ESMs from the Sixth Phase of the Coupled Model Intercomparison Project (CMIP6). For each ESM, we train on a single ensemble member across scenarios and evaluate the emulator performance using simulations with historical and SSP5-8.5 forcing. We show that the framework captures grid point specific precipitation characteristics, such as variability, trend and temporal auto-correlations. In addition, we find that emulated spatial (cross-variable) characteristics are consistent with that of ESMs. The framework is also able to capture compound hot-dry and cold-wet extremes, although it systematically underestimates their occurrence probabilities. The emulation of spatially explicit, coherent monthly temperature and precipitation timeseries is a major step towards the representation of impact-relevant variables of the climate system in a computational efficient manner.

https://doi.org/10.5194/egusphere-2024-278
Preprint. Discussion started: 13 May 2024
© Author(s) 2024. CC BY 4.0 License.

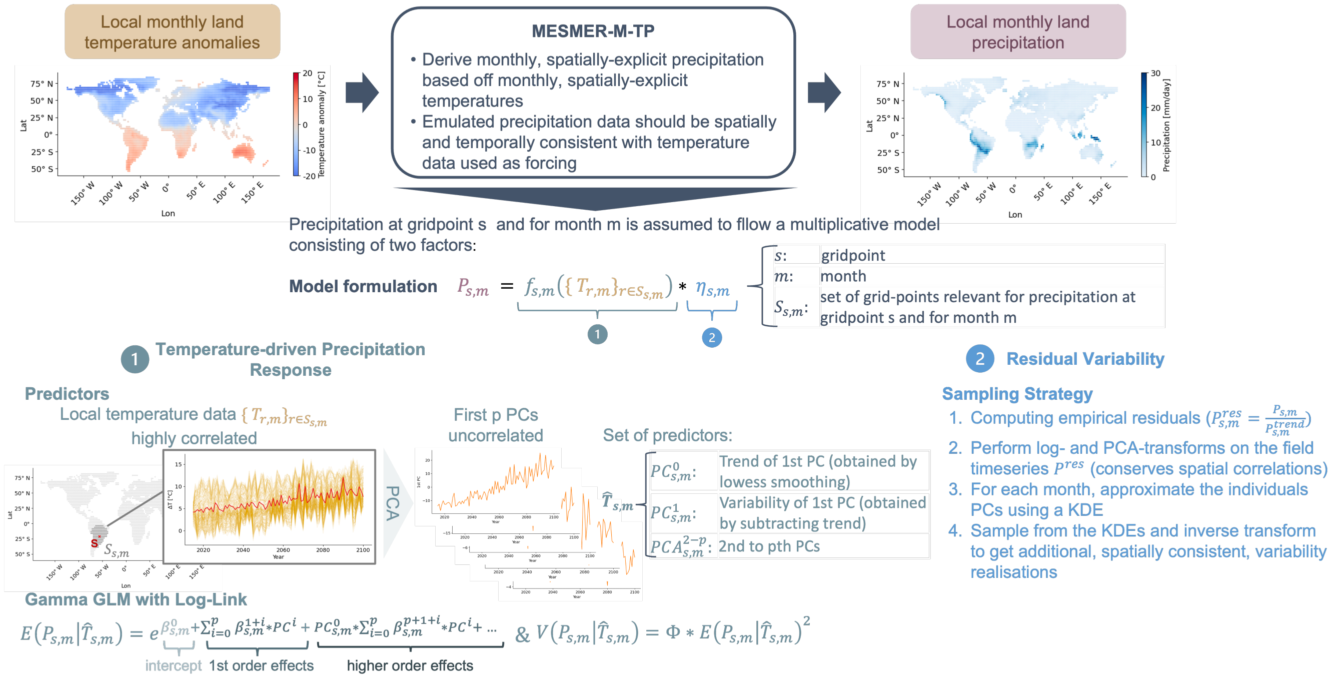

1 Introduction

Earth System Models (ESM) are process-based models built off physical equations that govern the dynamic and thermodynamic process of the Earth system (e.g., Schneider et al., 2017). Their physically based modelling approach makes ESMs invaluable for understanding and explaining the impacts of human activities on the global climate. At the same time, the modelling approach is computationally expensive - generating a single ESM simulation for the Sixth Phase of the Coupled Model Intercomparison Project (CMIP6) takes weeks to months to complete (e.g., Balaji et al., 2017). This limits the number of times any ESM can be run. However, studying a broad variety of different emission scenarios along with estimating associated uncertainties and sampling natural variability traditionally requires running an ESM many times (Lehner et al., 2020; Maher et al., 2021).

Emulators of ESMs are runtime efficient models that approximate specific outputs of an ESM using statistical methods. An emulator (in this paper the term emulator always refers to ESM emulators) is trained to approximate relationships between a set of predictor variables and selected target variable(s) from existing ESM data, which can then be applied to new predictor data. The temporal and spatial properties of the emulated target variable(s) should, ideally, not be statistically distinguishable from those of the actual ESM output. Emulators typically focus on a small set of key target variables, which reduces dimensionality and saves computational time as well as storage. This is a sensible choice as for many downstream applications of ESM data only a small set of climatic variables is of interest: for example, the Large Ensemble output of the Community Earth System Model (CESM-LE) consists of 1168 climatic variables of which 64% are virtually never downloaded while 14% contribute to over 90% of downloads (Edwards et al., 2019). Emulators can generate thousands of realisations of ESM-like

https://doi.org/10.5194/egusphere-2024-278
Preprint. Discussion started: 13 May 2024
© Author(s) 2024. CC BY 4.0 License.

data, thereby overcoming the limitations of only having a small number of ESM realisations. As such, ESMs and emulators are complementary.

A number of such emulation frameworks of varying complexity exist. Some frameworks aim to approximate the mean trend of a single variable (e.g., Tebaldi and Arblaster, 2014, and references therein), others also emulate variability as either a stationary (e.g., Link et al., 2019) or a non-stationary (e.g., Nychka et al., 2018) process. Recent approaches target the simultaneous emulation of multiple variables to also correctly mimic cross-variable covariance structures (e.g., Tebaldi et al., 2022; Edwards et al., 2019; Liu et al., 2023). Emulators can also target different spatial and temporal scales (e.g. yearly: Beusch et al. (2020) or monthly: Nath et al. (2022)). Emulators often use global mean temperature (GMT) as a predictor variable (e.g., Quilcaille et al., 2022) and some use additional predictors, such as ocean heat uptake, land-sea temperature contrast or time-shifted GMT (e.g., Herger et al., 2015; Beusch et al., 2022).

In this study, we focus on generating emulations of monthly gridded land precipitation from monthly gridded land temperatures, while aiming to represent the covariance structure between the two variables. Temperature and precipitation are two of the most important climatic variables and are needed as input variables for most impact models (Lange, 2019).

There are already emulators targeted at jointly emulating temperature and precipitation. For example, Tebaldi et al. (2022) built their emulator STITCHES using resampling methods. They pool together all available data from any scenario, re-arrange it using constraints on global mean temperature and then ‘stitch" it back together. This enables STITCHES to generate multivariate, spatially-resolved emulations. However, the quality of the emulator is constrained by the amount of available ESM training data and does not perform ideally when data is under-representative. Link et al. (2019) have extended their temperature emulator, fldgen1.0, to also model precipitation (fldgen2.0; Snyder et al., 2019). Their framework relies on capturing the signal's mean response using pattern scaling (Tebaldi and Arblaster, 2014, and references therein) and then adding a variability term. The variability term possesses the spatio-temporal (cross-)correlations and is generated by decomposing the original ESM signal into its principal components (PCs), applying a Fourier transformation to the PCs, applying random phase shifts and then back-transforming. Fldgen2.0 has been developed and tested for yearly data and implicitly assumes stationarity in the variability of temperature and precipitation. Recently, Liu et al. (2023) developed a precipitation emulator, PrEMU, that targets the emulation of monthly gridded precipitation starting from monthly gridded temperatures. Their approach is able to deterministically reconstruct 70% of the variance in global land average precipitation. However, PrEMU does not offer to emulate the remaining variance and cross-variable covariances have not been verified.

In this study, we present a novel approach that aims at fully emulating land precipitation fields at monthly resolution given a time series field of land temperatures, while especially approximating the cross-variable covariance structures. We show that the emulation framework resembles ESM output well and even captures monthly compound-extremes. Our emulator, called MESMER-M-TP, serves as an additional module within the MESMER (Modular Earth System Model Emulator with spatially Resolved output) framework (Beusch et al., 2020). MESMER has originally been designed to approximate grid-point level annual mean temperatures changes as a function of global mean temperature change, while explicitly accounting for spatial and temporal variability (Beusch et al., 2020). This approach has since been extended to also represent selected extreme weather indicators (MESMER-X), and key impact relevant variables such as fire weather and soil moisture (Quilcaille et al., 2022, 2023). A temporal downscaling module to emulate monthly climate output has also been successfully implemented (MESMER-M) (Nath et al., 2022). We here provide a module that can be coupled to MESMER-M temperature output (or to output from other emulators of monthly local temperatures) to generate bivariate temperature and precipitation emulations. The core of the approach employs Generalised Linear Models (GLMs) (Dobson and Barnett, 2018). Our framework is easily extendable to other variables that follow distributions within the exponential family and it allows for non-stationary variance functions.

This study is structured as follows: First, the methodological emulation framework is introduced in Sect. 2. Second, we describe how the suggested methodology is applied to the ESM data in Sect. 3. To this end, we introduce the data set (Sect. 3.1), give an overview on how the methodology is applied to the data (Sect. 3.2) and describe the validation of the emulation framework (Sect. 3.3). Next, we present our results in Sect. 4. The results section contains exemplary emulation output and validation metrics. Lastly, we summarise and discuss findings in Sect. 5. In addition, this paper comes with an extensive Appendix C that is mainly concerned with coupling MESMER-M-TP to an emulator that generates temperature data. In the appendix, validation and uncertainty estimations are carried out for the coupled emulation chain.

2 Emulator Description

2.1 Notation

T and P denote the spatially explicit monthly temperature and precipitation fields. We introduce the subscripts s, m and y, such that $p_{s,m,y}$ ($t_{s,m,y}$) is the precipitation (temperature) value at location s, for month m and year y. We set $m = 1$ as January and $m = 12$ as December. P (and T) can be expressed as a 2-dimensional matrix with columns corresponding to spatial locations and rows referring to specific month-year combinations:

$$P = \begin{pmatrix} p_{s_1,1,y_1} & p_{s_2,1,y_1} & \cdots & p_{s_l,1,y_1} \\ p_{s_1,2,y_1} & p_{s_2,2,y_1} & \cdots & p_{s_l,2,y_1} \\ \vdots & \vdots & \ddots & \cdots \\ p_{s_1,12,y_1} & p_{s_2,12,y_1} & \cdots & p_{s_l,12,y_1} \\ p_{s_1,1,y_2} & p_{s_2,1,y_2} & \cdots & p_{s_l,1,y_2} \\ \vdots & \vdots & \ddots & \cdots \\ p_{s_1,12,y_k} & p_{s_2,12,y_k} & \cdots & p_{s_l,12,y_k} \end{pmatrix}, \qquad (1)$$

where l denotes the number of spatial locations and k the number of years. The matrix has dimensions $dim(P) = (12 * k) \times l$. The precipitation timeseries at location s is the row-vector $P_s = (p_{s,1,y_1}, p_{s,2,y_1}, \dots, p_{s,12,y_1}, p_{s,1,y_2}, \dots, p_{s,12,y_k})^T$, where the superscript T refers to the transpose. We define the gridpoint and month specific precipitation as the timeseries consisting of precipitation samples from the same month over different years: $P_{s,m} = (p_{s,m,y_1}, p_{s,m,y_2}, ..., p_{s,m,y_k})^T$, meaning $P_{s,m}$ contains every 12th entry of P_s. All definitions work analogously for monthly temperatures.

https://doi.org/10.5194/egusphere-2024-278
Preprint. Discussion started: 13 May 2024
© Author(s) 2024. CC BY 4.0 License.

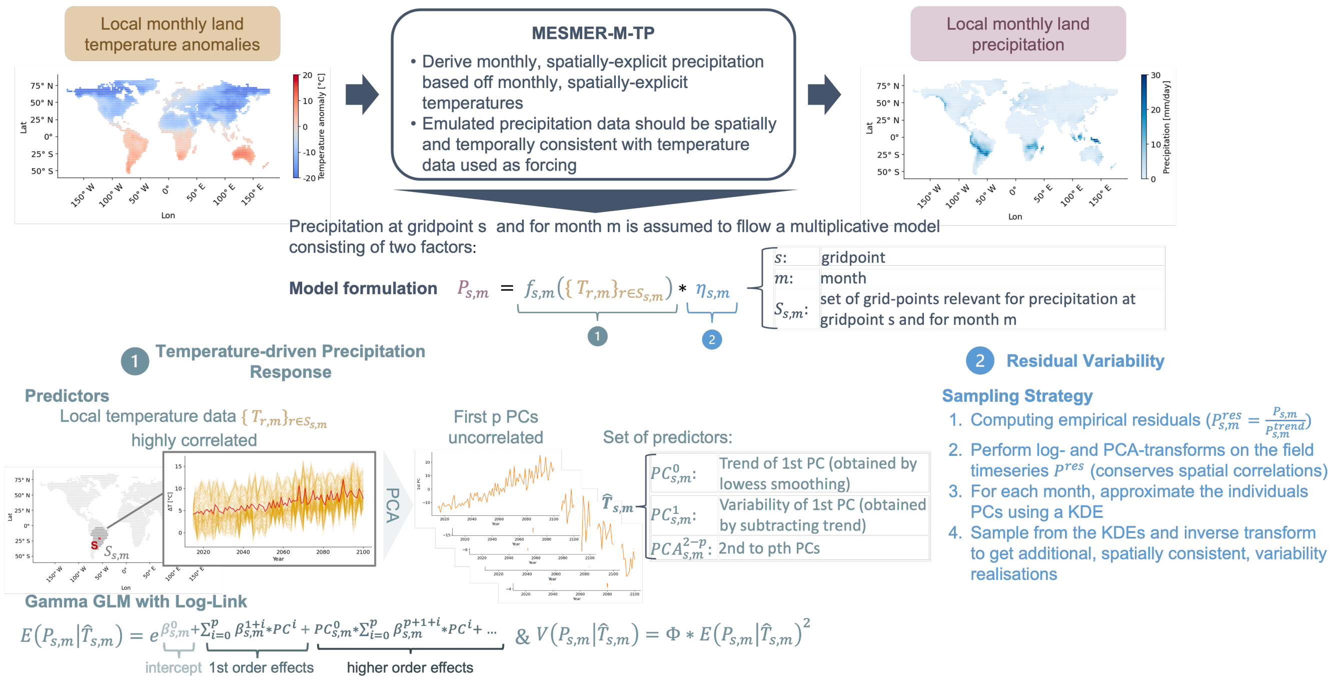

Figure 1. Schematic overview of our modelling approach. Precipitation is decomposed into a temperature-driven contribution and a contribution independent of temperature. We exploit local temperature information and the framework of Gamma GLMs to reconstruct precipitation signals for each location and month. We then compute the empirical residuals and after applying a log and a PCA transform to disentangle spatial correlations, we approximate the residuals individually by using a KDE. The framework is described in more detail in Sect. 2

2.2 General Approach

The goal of the emulator is to derive monthly, spatially-explicit precipitation based on monthly, spatially-explicit temperatures. In particular, the emulated precipitation data should be spatially and temporally consistent with the temperature data. To this end, we suggest a multiplicative framework that can be summarised as

$$P_{s,m} = \underbrace{f_{s,m}\left(\{T_{r,m}\}_{r\in S_{s,m}}\right)}_{1} * \underbrace{\eta_{s,m}}_{2}, \tag{2}$$

where the local precipitation at gridpoint s and for month m, $P_{s,m}$, is defined by two terms. (1) By the deterministic temperature-driven precipitation response. We assume that a large fraction of $P_{s,m}$ can be constructed from local temperature information. Let $S_{s,m}$ be the set of spatial locations with temperature timeseries that may contain useful information for reconstructing $P_{s,m}$. We then use $\{T_{r,m}\}_{r\in S_{s,m}}$ to build a 2-dimensional predictor matrix $\mathbf{X}_{s,m}$. We assume that $\mathbf{X}_{s,m}$ relates to $P_{s,m}$ via the response function $f_{s,m}$. Note that $f_{s,m}$ acts independently on each gridpoint and for each month (see Sect. 2.3.2). And (2) by a stochastic, multivariate noise term, η. η is used to approximate the fraction of the natural variability that can not be reconstructed from temperature information alone and thus appears random in our modelling framework. We assume that the precipitation residuals still possess information across locations and months, but are independent of temperature. η is evaluated at gridpoint s and for month m.

The suggested framework is equivalent to assuming an additive model for the logarithm of precipitation which is a common choice when modelling precipitation (e.g., Snyder et al., 2019; Gudmundsson and Seneviratne, 2016; McCullagh, 2019).

2.3 Temperature-driven Precipitation Response

The aim of the temperature-driven precipitation response is to capture the fraction of the precipitation signal that is deterministically derivable from temperature data. We do not assume a causal relationship here. Rather, the motivation is to provide for a consistent multivariate extension. To this end, we assume that temperature is a good predictor for the general trend in the precipitation signal as well as parts of the variability. In order to capture both contributions simultaneously, we rely on the framework of GLMs (e.g. Dobson and Barnett, 2018; McCullagh, 2019). A GLM is a generalisation of ordinary linear regression and is applicable to any dependent variable that follows a specific distribution within an exponential family relative to the predictor variable(s). The basic assumption is that the dependent variable is related to a linear combination of the independent variables via a link function.

2.3.1 A GLM for Precipitation

To apply the GLM framework to precipitation, we assume that $P_{s,m}$ follows a Gamma distribution with shape parameter $k_{s,m}$ and scale parameter $\Theta_{s,m}$ conditioned on a set of temperature predictors accounting for the local and global temperature conditions, $\mathbf{X}_{s,m}$ (see Sect. 2.3.2). Precipitation is continuous and non-negative while the Gamma distribution is strictly positive. By replacing zero precipitation values with a small threshold for quasi-zero, the condition for the Gamma distributions can be met. We choose a logarithmic link function, $g = log$, such that the inverse link function is the exponential function, $g^{-1} = e$. The model formulation then reads as follows:

$$E(P_{s,m}|\mathbf{X}_{s,m}) = e^{\mathbf{X}_{s,m}*\beta_{s,m}} + \text{higher order terms} = \mu_{s,m} \tag{3}$$

where $E(P_{s,m}|\mathbf{X}_{s,m})$ is the expected value of $P_{s,m}$ conditioned on the predictors $X_{s,m}$, $\mu_{s,m}$ is the expected value of the Gamma distribution, and $\beta_{s,m}$ is a vector of linear coefficients (see Sect. 3.2 for details on the higher order terms). The mean of a Gamma distribution can also be expressed using its scale and shape parameters:

$$\mu_{s,m} = k_{s,m} * \Theta_{s,m}. \tag{4}$$

Equally, the variance of a Gamma distribution can be expressed as:

$$var_{s,m} = k_{s,m} * \Theta^2_{s,m}. \tag{5}$$

In GLMs, the shape parameter is usually held constant while the scale parameter is varied. Therefore, by combining Eq. 4 and 5 we get the variance function for the Gamma GLM,

$$V(P_{s,m}|\mathbf{X}_{s,m}) = \Phi_{s,m} * E(P_{s,m}|X^T_{s,m})^2, \tag{6}$$

where $\Phi_{s,m}$ is called the dispersion and is a constant and $V(P_{s,m}|\mathbf{X}_{s,m})$ is the variance of $P_{s,m}$ conditional on the predictors $\mathbf{X}_{s,m}$. As the conditional mean of the precipitation distribution is changing with the background climate, this variance-mean relationship offers to model non-stationary behaviour in the precipitation response. At the same time, imposing the variance function of a Gamma GLM is a strong assumption that may not hold true at all locations. However, using a Gamma GLM to model precipitation has been shown to yield good approximations in other studies (George et al., 2016; Hauser et al., 2017; Chandler, 2020) and in Sect. 3.3, we empirically validate our choice.

2.3.2 The Predictor Matrix $\mathbf{X}_{s,m}$

Precipitation is a complex climatic variable that depends on many factors such as water availability, temperatures or the terrain (Allen and Ingram, 2002; Trenberth et al., 2003; Tabari, 2020). As the goal is to reconstruct precipitation signals using temperature information only, we try to exploit local temperature information as much as possible. We assume that, in order to construct $P_{s,m}$, temperature information at all gridpoints r in proximity to s is relevant. We denote $S_{s,m}$ as the set of n spatial locations that are closest to s and we assume that all $\{T_{r,m}\}_{r\in S_{s,m}}$ are relevant predictors for $P_{s,m}$. As the timeseries' in $\{T_{r,m}\}_{r\in S_{s,m}}$ are highly correlated, we perform a PCA transform and only keep the first p components. That is, we project $\{T_{r,m}\}_{r\in S_{s,m}}$ onto its p-dimensional Eigenspace spanned by the vectors $\{PCA^i_{s,m}\}_{i\in\{0,\dots,p-1\}}$. The first principal component, $PCA^1_{s,m}$, is now expected to contain a strong trend. As precipitation may scale differently with temperature information on different timescales, we decompose $PCA^0_{s,m}$ into a trend and a variability term. The trend term is derived by LOWESS smoothing consistent with the methodology in Beusch et al. (2022). This leaves us with the set $\hat{T}_{s,m} = \{PCA^{0,trend}_{s,m}, PCA^{0,var}_{s,m}, PCA^1_{s,m}, PCA^1_{s,m}, \dots, PCA^{p-1}_{s,m}\}$ as a set of feasible predictors. $\mathbf{X}_{s,m}$ is then constructed by using the set $\hat{T}_{s,m}$ as row vectors and by adding column of ones to allow for a constant intercept:

$$\mathbf{X}_{s,m} = \begin{pmatrix} 1 & PCA^{0,trend}_{s,m,y_0} & PCA^{0,var}_{s,m,y_0} & PCA^1_{s,m,y_0} & PCA^2_{s,m,y_0} & \dots & PCA^{p-1}_{m,s,y_0} \\ 1 & PCA^{0,trend}_{s,m,y_1} & PCA^{0,var}_{s,m,y_1} & PCA^1_{s,m,y_1} & PCA^2_{s,m,y_1} & \dots & PCA^{p-1}_{m,s,y_1} \\ \vdots & \vdots & \vdots & \vdots & \vdots & \ddots & \vdots \\ 1 & PCA^{0,trend}_{s,m,y_k} & PCA^{0,var}_{s,m,y_k} & PCA^1_{s,m,y_k} & PCA^2_{s,m,y_k} & \dots & PCA^{p-1}_{m,s,y_k} \end{pmatrix}. \tag{7}$$

The model design also offers to include higher order effects by, for example, including $\mathbf{X}^2_{s,m}$ as additional predictors or including pairwise interactions between predictors. Including higher-order effects is a calibration choice and is discussed in Sect. 3.2.

2.4 Residual Variability

We define the residual variability of the precipitation signal as the fraction of precipitation that cannot be derived from temperatures:

$$P^{res}_{s,m} = P_{s,m}/f_{s,m}(X^T_{s,m}) \tag{8}$$

https://doi.org/10.5194/egusphere-2024-278
Preprint. Discussion started: 13 May 2024
© Author(s) 2024. CC BY 4.0 License.

We assume that $P^{res}_{s,m}$ is independent of temperature, but dependent on all other precipitation residuals. That is, the field P^{res} still possesses spatial correlations, for example, residuals between two gridcells in proximity are likely similar. As a Gamma-GLM does not contain any explicit assumptions about the distribution of the empirical residuals, we are relying on approximating the empirical distribution of the residuals and then sampling from them. To this end, we first apply a log transform to the residuals to avoid difficulties with potentially modelling negative values. To resolve the spatial dependencies across precipitation residuals, a PCA transform is applied to the residuals. For each month, the distribution of the resulting PCs is empirically estimated using a Kernel Density Estimation (KDE) with a Gaussian Kernel and bandwidth parameter h_m. In order to generate additional, random variability realisations, we draw new samples from the KDE, employ the inverse PCA transform and then the inverse log transform.

2.5 Model Parameters

To summarise the above approach: We first construct the gridpoint and month specific predictor matrix $\mathbf{X}_{s,m}$ using local temperature information. This offers two calibration parameters: (i) the number of the n-closest spatial locations that still influence precipitation at location s and (ii) the number of PCA components, p, that should be kept as predictors. The matrix $\mathbf{X}_{s,m}$ has p+2 columns (the first PC is divided into a trend and a variability contribution and we have a column of ones to allow for a constant offset), leaving us with p+2 parameters for each grid point and month (the parameters are encompassed in the coefficient vector $\beta_{s,m}$). $\beta_{s,m}$ is fitted using the framework of a Gamma GLM and a log-likelihood estimation. As the residuals of a Gamma GLM do not have a pre-described functional form, we are approximating the residuals using a KDE that relies on a smoothing parameter (also called bandwidth), h_m.

3 Emulator Application

3.1 Data

The emulator is trained on monthly mean temperature and monthly mean precipitation data from CMIP6 experiments (Eyring et al., 2016) of 24 different ESMs (see Table A1 in Appendix A). In this study, the term temperature refers to temperature anomalies relative to the period 1850-1900 while precipitation refers to absolute precipitation. The ESM data went through a centralised pre-processing that includes the interpolation to a common $2.5° \times 2.5°$ latitude-longitude grid and was obtained from the CMIP6 next generation archive (Brunner et al., 2020). As variables are emulated over land only, grid cells with a land area coverage of less than a third are filtered out, resulting in 2652 land grid points. Monthly precipitation data can contain zero values and in some cases very small negative numerical residuals. Therefore, for each ESM, a cut-off for quasi-zero is introduced by replacing zero and negative values with half of the smallest non-negative precipitation value found in the entire dataset. Data from five scenarios (SSP1-1.9, SPP1-2.6, SPP2-4.5, SPP3-7.0, SSP5-8.5) and the historical simulations are considered (O'Neill et al., 2016). Not all 24 models provide temperature and precipitation data for each SSP (see Table A1 in A). For each ESM, the emulator is trained independently based on a single ensemble member across all available SSPs. The

https://doi.org/10.5194/egusphere-2024-278
Preprint. Discussion started: 13 May 2024
© Author(s) 2024. CC BY 4.0 License.

historical simulation and the SSP5-8.5 scenario of the remaining ESM ensemble members are used for evaluating the emulator performance and are referred to as validation runs. A special focus is put on the three models with the highest number of validation runs: ACCESS-ESM1-5, CanESM5 and MPI-ESM1-2-LR. These three models offer at least 30 ensemble members each which allows us to compare ensemble statistics and, in particular, extreme event distributions.

MESMER-M-TP has been designed as a module that can be coupled to existing temperature emulators. To additionally evaluate the emulator performance and the propagation of uncertainties in this context, the trained emulator is coupled to emulated monthly temperatures of the historical simulation and the SSP5-8.5 scenario. The emulated temperature dataset was specifically generated for this study and is described in Appendix C1.

3.2 Calibration

The methodological framework described in Sect. 2 offers a few adjustable parameters (see Sect. 2.5) for both, the temperature-driven precipitation response module and the residual variability module. As part of the temperature-driven precipitation response, $P_{s,m}$, is reconstructed from information in the n closest temperature timeseries, $\{T_{r,m}\}_{r \in S_{s,m}}$ with $|S_{s,m}| = n$. For simplicity and comparability, we assume that n is constant across models, months and gridpoints. Therefore, $S_{s,m}$ only depends on the spatial location and reduces to S_s. We find that across months and models, the strongest correlations between the variability in temperature and the variability in precipitation occur in almost 80% of the cases within the closest 150 gridpoints. Thus we set $n = 150$, such that we can derive precipitation based on the 150 closest temperature locations. In addition, choosing a comparably small number of predictors offers to include more direct links to local modes of variability. As the set of $\{T_{r,m}\}_{r \in S_s}$ are highly correlated, we apply a PCA transformation prior to using them as independent variables for the GLM (see Sect. 2.3.2). The amount of explained variance in each PC falls off rapidly over the first five PCs and strives towards zero with increasing component number. To include as much information as possible, while not inflating the model, we set $p = 8$. In addition, we include contributions from 1st order interaction terms between the trend in the 1st PC and all other PCs. This allows for the relative importance of the PCs to vary with the trend in local temperatures. Lastly, we set the parameters of the residual variability module. We apply a PCA on the precipitation residuals in order to resolve spatial correlations and treat the PCs independently. We keep 98% of the variability in the original residual signals. The bandwidth of the KDE was chosen via k-fold cross validation and was mostly constant across months and models. To reduce computational complexity, we have set $h_m = 0.1$ as a global parameter.

3.3 Validation

The validation framework consists of two steps: (1) Evaluating the emulator's performance when it emulates precipitation based on actual ESM temperatures and (2) evaluating the model's performance when it emulates precipitation based on emulated temperatures. The first evaluation step captures the direct error in the emulation framework while the second step also captures the propagation of uncertainties from one emulator to another. Results for the former are shown in Sect. 4, while results for the latter are shown in Sect. C. The evaluation procedure and result metrics are the same in both cases and described in the following.

https://doi.org/10.5194/egusphere-2024-278
Preprint. Discussion started: 13 May 2024
© Author(s) 2024. CC BY 4.0 License.

The emulator is trained on one ensemble member across all available scenarios (see Sect. 3.1). Temperature data from all remaining ensemble members is used to generate emulated precipitation data for the first evaluation step (for the second evaluation step, we use the temperature dataset described in Sect. C1 as forcing). Both emulation datasets are assessed against actual ESM precipitation data from all remaining ensemble members for the historical period (1850-1950) and the projections from the high warming scenario SSP5-8.5 (2015-2100) independently. The time intervals and the scenario are chosen such that the emulator's behaviour in a stable period with limited climate change and its behaviour under an extreme, high-warming scenario can be equally analysed. As the three models ACCESS-ESM1-5, CanESM5 and MPI-ESM1-2-LR are the only models that offer a large number of additional ensemble members for evaluation (30+), we focus on validating the emulation approach using these three models and only schematically show results for all other models. In addition, we base our evaluation on the SREX regions (Seneviratne et al., 2012) with an emphasis on four regions that represent a diverse set of geographies and precipitation trends: Central North America (CNA), Northern Europe (NEU), Central Africa (CAF), South East Asia (SEA) (see also Fig. A1). We validate the following properties:

(1) **Inter-annual trend and variability of precipitation.** We aim at verifying the emulated estimates of inter-annual trend as well as of year-to-year variability in $P_{s,m}$ across regions. To this end, ESM and emulated (EMU) data are aggregated by SREX region. Next, all quantiles between the 1st and 99th quantile are computed in steps of one and compared against one another for both the historic and the future period. In addition, we compute quantile deviations for the 10th, median and 90th quantile for each region (see Nath et al., 2022; Beusch et al., 2020). The Gamma GLM is mainly responsible for correctly estimating the trend in $P_{s,m}$, while the residual variability module determines the variability in $P_{s,m}$. Therefore, the deviations allow to draw conclusions on the performance of both models.

(2) **Month-to-month relationships of precipitation.** The emulator was fitted for each month independently and only implicitly inherits month-to-month relationships from the temperature data. Therefore, we verify the month-to-month relationships using lagged auto-correlations. At each grid point and for each ensemble member, the correlation between the precipitation timeseries and a temporally shifted version of the same precipitation timeseries is computed. The correlation coefficient is computed for each ESM run and each EMU run individually and then averaged to obtain a single ESM/EMU value per grid-point.

(3) **Spatial precipitation structure.** The spatial structure in the precipitation signal is partially inherited form the spatial structure of the temperature field and partially explicitly enforced through the sampling strategy of the residuals. We verify that the joint use of the GLM and the KDE produces spatially coherent precipitation fields. To this end, we compute the month specific cross-correlation matrix between precipitation timeseries at different gridpints for each ensemble member. More precisely, for a given month and ensemble member, we compute the correlation between precipitation at any given gridpoint and precipitation at all other grid points. As we have 2652 grid points this results in a correlation matrix of dimension (2652, 2652) whose entry (i, j) describes the correlation between $P_{s_i,m}$ and $P_{s_j,m}$. We compute the ensemble-mean of the correlation matrices and compare emulated estimates against ESM estimates.

(4) **Spatial precipitation-temperature cross-variable correlations.** The GLM relies on exploiting local temperature information to reconstruct precipitation. Verifying that spatial cross-variable correlations are approximated well, verifies the

https://doi.org/10.5194/egusphere-2024-278
Preprint. Discussion started: 13 May 2024
© Author(s) 2024. CC BY 4.0 License.

modelling approach and is important for downstream applications that rely on spatially and temporally consistent temperature and precipitation data. We verify the cross-variable statistics by computing the cross-correlation matrix between the precipitation and the temperature field for each month and for each ensemble member individually. Similar to (3), for a given month, precipitation at any gridpoint is correlated with temperature at any other grid points. This results in a correlation matrix of dimension (2652, 2652) whose entry (i, j) describes the correlation between $P_{s_i,m}$ and $T_{s_j,m}$.

(5) **Compound temperature-precipitation extremes.** As the mechanistic processes that govern the occurrence of extremes are very different to the processes that determine long-term trends, verifying mean temperature-precipitation correlations alone is not enough to draw conclusions about the joint distributions of the tails. Therefore, we verify compound extremes individually. At each grid point, the 10th and 90th quantiles of temperature and precipitation are computed across ensemble members for ESM and EMU. To assess hot-dry extremes, we count the number of times a projection lies above the 90th temperature quantile and is simultaneously drier than the 10th precipitation quantile. Similarly, for cold-wet extremes, we count the number of times a projection is cooler than the 10th temperature quantile and simultaneously wetter than the 90th precipitation quantile. We then compute the mean across ESM and EMU estimates and scale the count to the number of events that would happen during the course of 100 years.

4 Results

The result section is divided into two parts. In Sect. 4.1 we show all results that only concern precipitation characteristics, these are inter-annual trend, inter-annual variability, month-to-month relationships and the spatial structure of the precipitation signal (see properties (1)-(3) in Sect. 3.3). In Sect. 4.2, we show results concerning the joint characteristics of temperature and precipitation, these are the cross-correlation structure between temperature and precipitation as well as compound extremes (see properties (4) and (5) in Sect. 3.3). We mainly focus on validating results when temperature fields from actual ESMs are used as forcing. In Sect. C, we show all results from this section when the emulator is forced with emulated temperatures.

4.1 Precipitation Characteristics

As exemplary shown in Fig. 2 for January, the emulator performs well in capturing inter-annual trends as well as inter-annual variability across months and models. The emulator captures different precipitaton characteristics including quasi-stationarity (MPI-ESM1-2-LR in SEA), shift in the mean precipitation (CanESM5 SCA or ACCESS-ESM1-5 NEU) and a widening of the distribution resulting in an intensification of high precipitation months (ACCESS-ESM1-5 CAF) or an intensification of both high and low precipitation events (CanESM5 CAF). As shown in Fig. B1, the emulator performs similarly albeit slightly worse for the month of July. In July, there are strong inter-model differences between precipitation projections from different models (SCA and CAF), suggesting low predictive accuracy in the models. In some cases (ACCESS-ESM1-5 SEA and MPI-ESM1-2-LR CAF), the emulator systematically overestimates high-precipitation events (90th percentile).

In Fig. 3 and B1 we explore these deviations from ESM quantiles in more detail. Systematic deviations only become apparent in the upper tail of the distribution (above 95th quantile in January and above 90th quantile in July), where the emulated values

https://doi.org/10.5194/egusphere-2024-278
Preprint. Discussion started: 13 May 2024
© Author(s) 2024. CC BY 4.0 License.

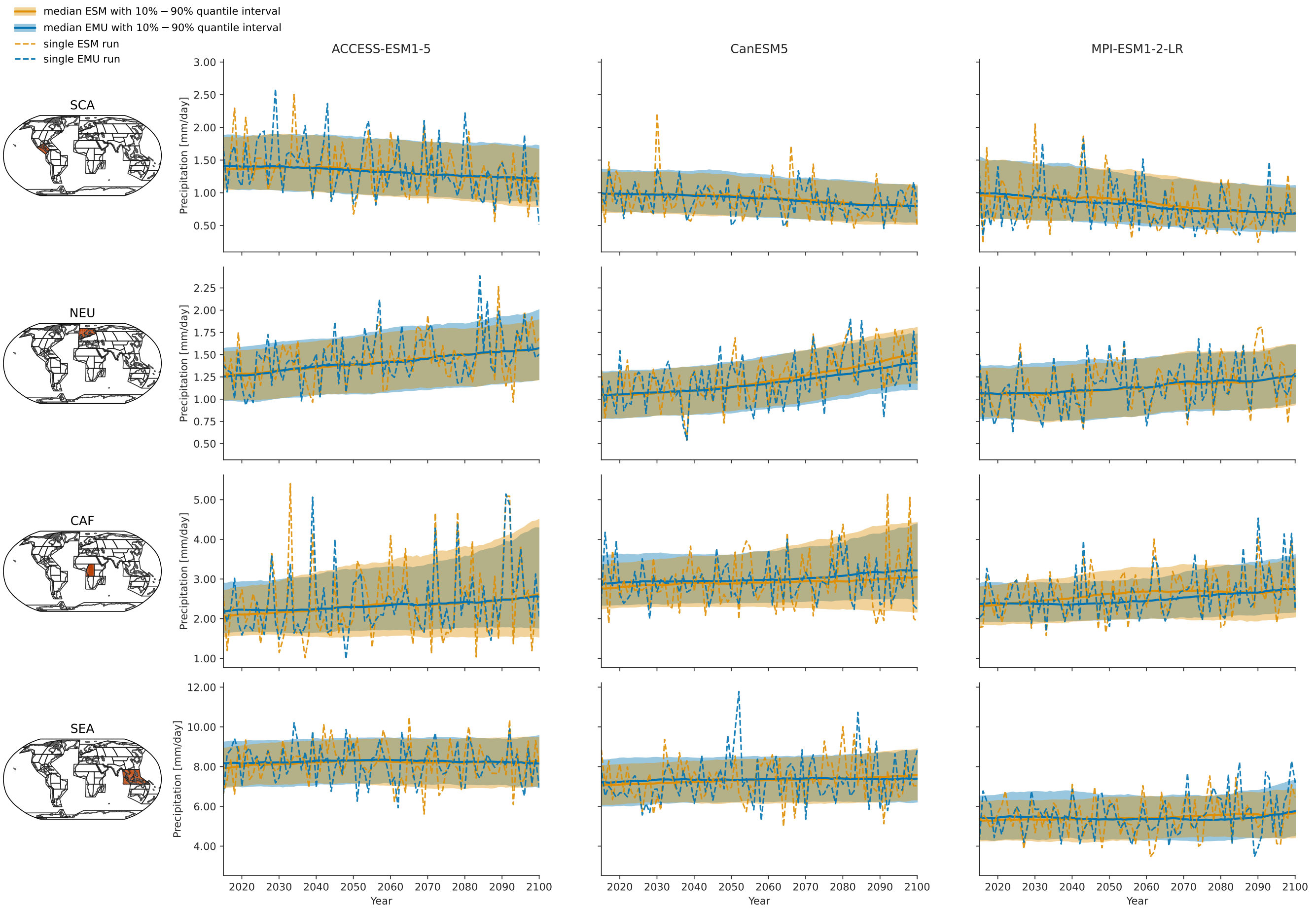

Figure 2. Timeseries of January precipitation from 2015-2100 for three different models (columns: ACCESS-ESM1-5, CanESM5, MPI-ESM1-2-LR) averaged over four SREX-regions(rows: SCA, NEU, CAF, SEA). The timeseries highlight the year-to-year trend and variability of January precipitation for SSP5-8.5. Orange/Blue line indicates the median ESM/EMU timeseries with shaded areas indicating 10%-90% quantile intervals. Orange/ Blue lines represent precipitation estimates of a single ESM/ EMU ensemble member. Note, the emulated timeseries was obtained using the ESM temperature field corresponding to the shown ESM precipitation timeseries as forcing.

https://doi.org/10.5194/egusphere-2024-278
Preprint. Discussion started: 13 May 2024
© Author(s) 2024. CC BY 4.0 License.

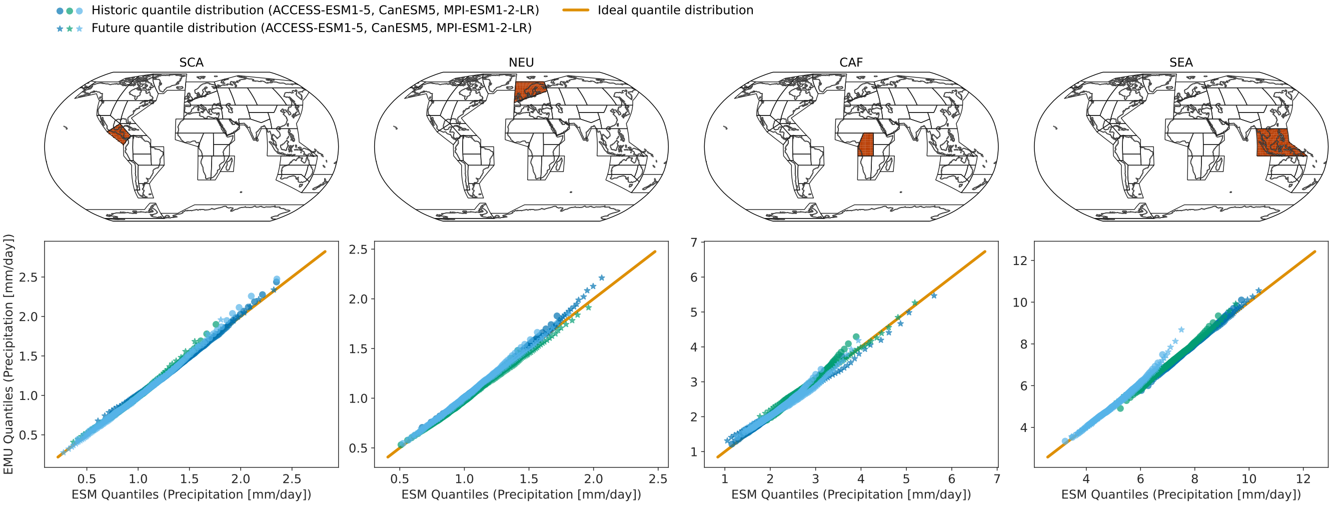

Figure 3. Quantiles (1st-99th in steps of one) derived from EMU data (y-Axis) scattered against estimates from ESM data (x-Axis) for four different regions (columns: SCA, NEU, CAF, SEA). The quantiles were estimated for the historical period (1850-1950) and the future period (2015-2100) independently and are displayed individually (circles vs. stars). Colours are used to distinguish data from different models. Quantiles were derived as described in Sect. 3.3.

tend to lie above those from ESMs (MPI-ESM1-2-LR in SEA for January and all models in NEU for July). The emulated quantiles are usually within ±10% of the ESM quantiles. In particular, the deviations are small compared to inter-model differences (January: SEA MPI-ESM1-2-LR compared to SEA ACCESS-ESM1-5). Our modelling framework implicitly suggests that non-stationarity in the variability of precipitation can only be inherited from non-stationarity in the temperature signals through the Gamma GLM. We do not account for potential non-stationarities in the residuals. The deviations in the tails of the distributions could indicate that this simplification is not strictly valid. We will discuss this in more detail in Sect. 5.

So far, we have only seen results for three models, for four regions and for precipitation emulations based on actual ESM temperature data. Figure 4 gives an indication for the model performance in other regions as wells as for the difference in performance when emulating based on emulated temperatures (see Beusch et al., 2020; Nath et al., 2022). The coupled emulator (see Fig. B3 right panel) generally performs well in regions where the direct emulation error is small (for example NZ or CNA) and usually suffers from stronger deviations whenever there already is a non-negligible error in the direct emulations (MPI-ESM1-2-LR GIC or WAF). In some cases, the coupled framework amplifies existing errors (ACCESS-ESM1-5 NWS and NES) or introduces new errors (ACCESS-ESM1-5 NSA). However, the performance is robust across forcing data and regions. We cannot estimate the direct emulation error for all 24 models due to a lack in available ESM data. In Fig. 5 we show the error in the coupled emulations for those models. The results are comparable to the deviations found for the three focus models. The emulation framework tends to slightly overestimate the 10th quantile and the 90th quantile, while it underestimates the 50th quantile (the same holds true for July, see Fig. 5). The underestimations of the 50th quantile over the historical period and the simultaneous overestimation of the 10th quantile could suggest that our modelling procedure struggles to adequately

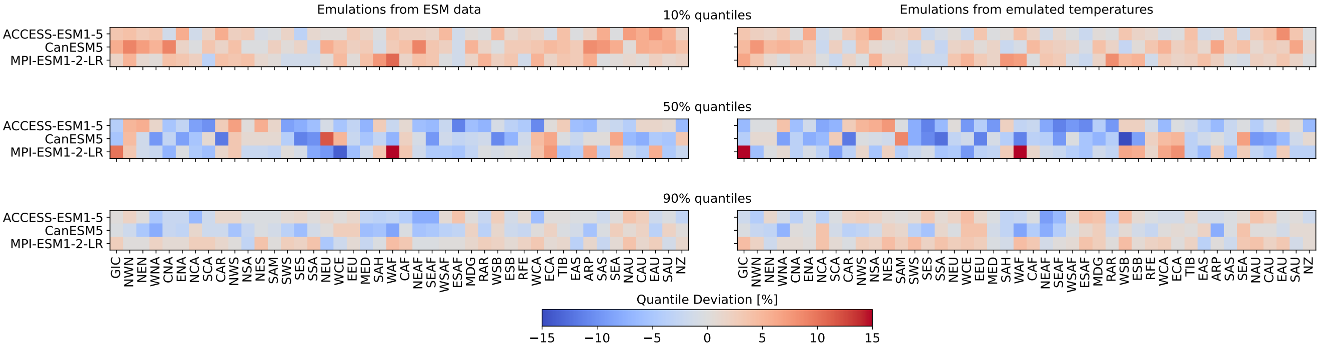

Figure 4. Regional deviations of January ESM precipitation from the 10% (top), 50% (middle) and 90% (bottom) quantiles of the emulations for the three focus models and across SREX regions (see Fig. A1 for a map of the SREX regions). Left: emulations based on ESM temperatures, right: emulations based on emulated temperatures. Quantile deviations were computed over the historical period. Red (blue) indicates that the emulations project higher (lower) values compared to ESM data (see Sect. 3.3).

disentangle the trend and variability contributions to the signal. In addition, there are some systematic overestimations of the 50th quantile in the July estimates (see Fig. B4), particularly in WAF, CAF and ARP.

We do not impose any constraints on month-to-month variations of precipitation, thereby implicitly assuming that precipitation inherits the correct temporal properties from the temperature data. In Fig. 6, we explore this simplified assumption using lagged auto-correlations. In general, lagged auto-correlations are captured very well and strongly decrease with increasing time-lag. The lag-1 correlations are slightly underestimated (in particular in MPI-ESM1-2-LR), but yield a consistent spatial pattern even without explicitly enforcing this structure. In particular, there is a high inter-model agreement on the temporal precipitation structure.

The spatial precipitation structure is partially constructed from the spatial correlations in the temperature field through the GLM, but mainly enforced relying on the sampling strategy of the variability module (see Sect. 2.4). In Fig. 7 we see that pairwise precipitation relationships are captured well by the model and note an overall good agreement across models and months (see Fig. B6). In particular, no systematic bias (for example a systematic over- or underestimation) is visible. This suggests that the residual variability module is well-suited to capture the spatial precipitation structures.

4.2 Joint Temperature-Precipitation Characteristics

As the precipitation emulations are built from local temperature data, we expect spatial cross-variable relationships between temperature and precipitation to be depicted well. In Fig. 8 we see that this is indeed the case. The emulator works particularly well if strong correlations are present (see also Fig. B5), while weaker correlations seem to be associated with a larger error. The strongest systematic errors (underestimation) occurs for MPI-ESM1-2-LR. Even though precipitation is constructed from temperature signals in a certain proximity, strong long-range correlations are also approximated (see Fig. B5). Noteworthy is the strong inter-model disagreement in the strength and direction of the temperature-precipitation correlations for July (see

https://doi.org/10.5194/egusphere-2024-278
Preprint. Discussion started: 13 May 2024
© Author(s) 2024. CC BY 4.0 License.

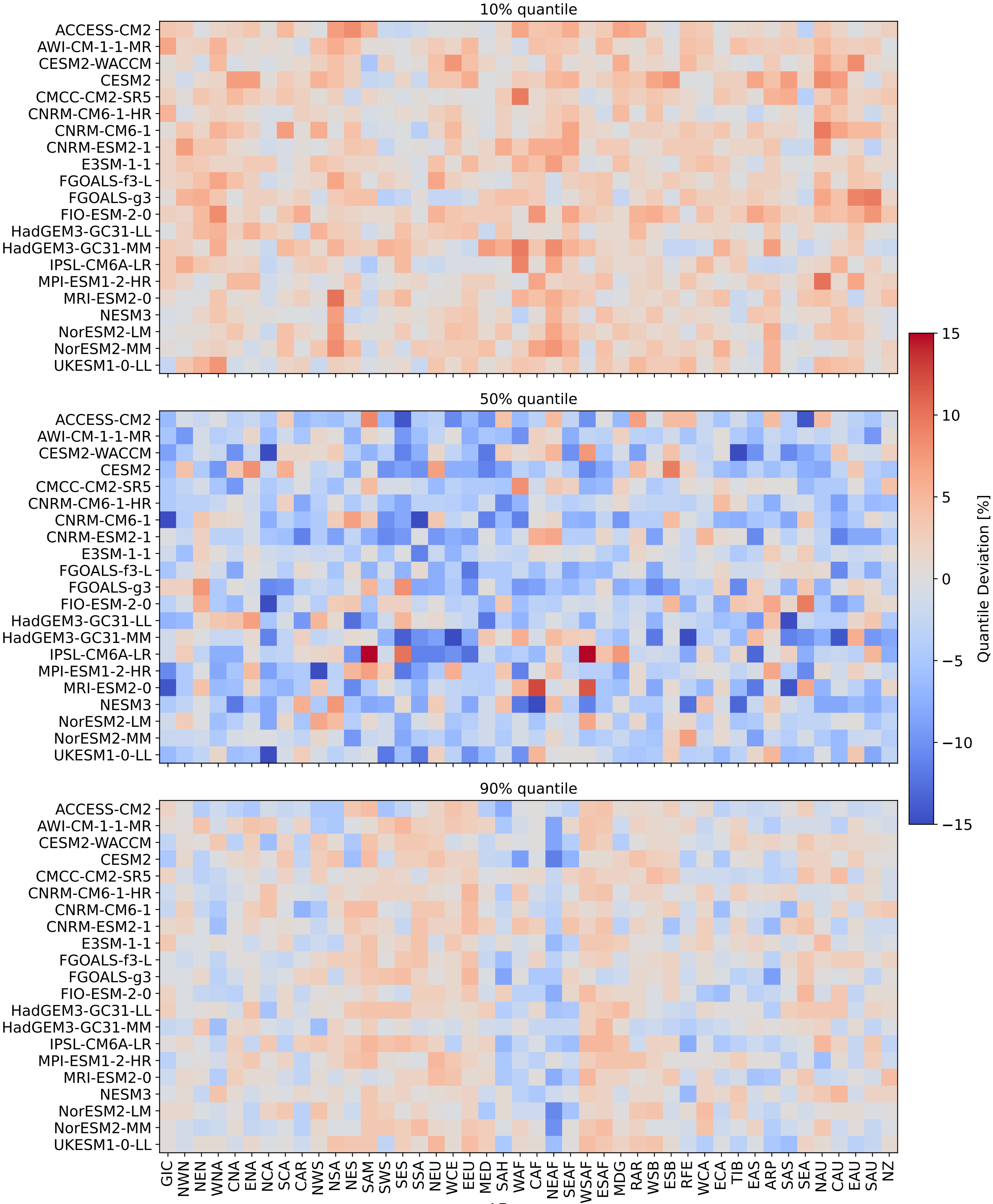

Figure 5. Same as the right panel in Fig. 4 but for the remaining 21 models.

https://doi.org/10.5194/egusphere-2024-278
Preprint. Discussion started: 13 May 2024
© Author(s) 2024. CC BY 4.0 License.

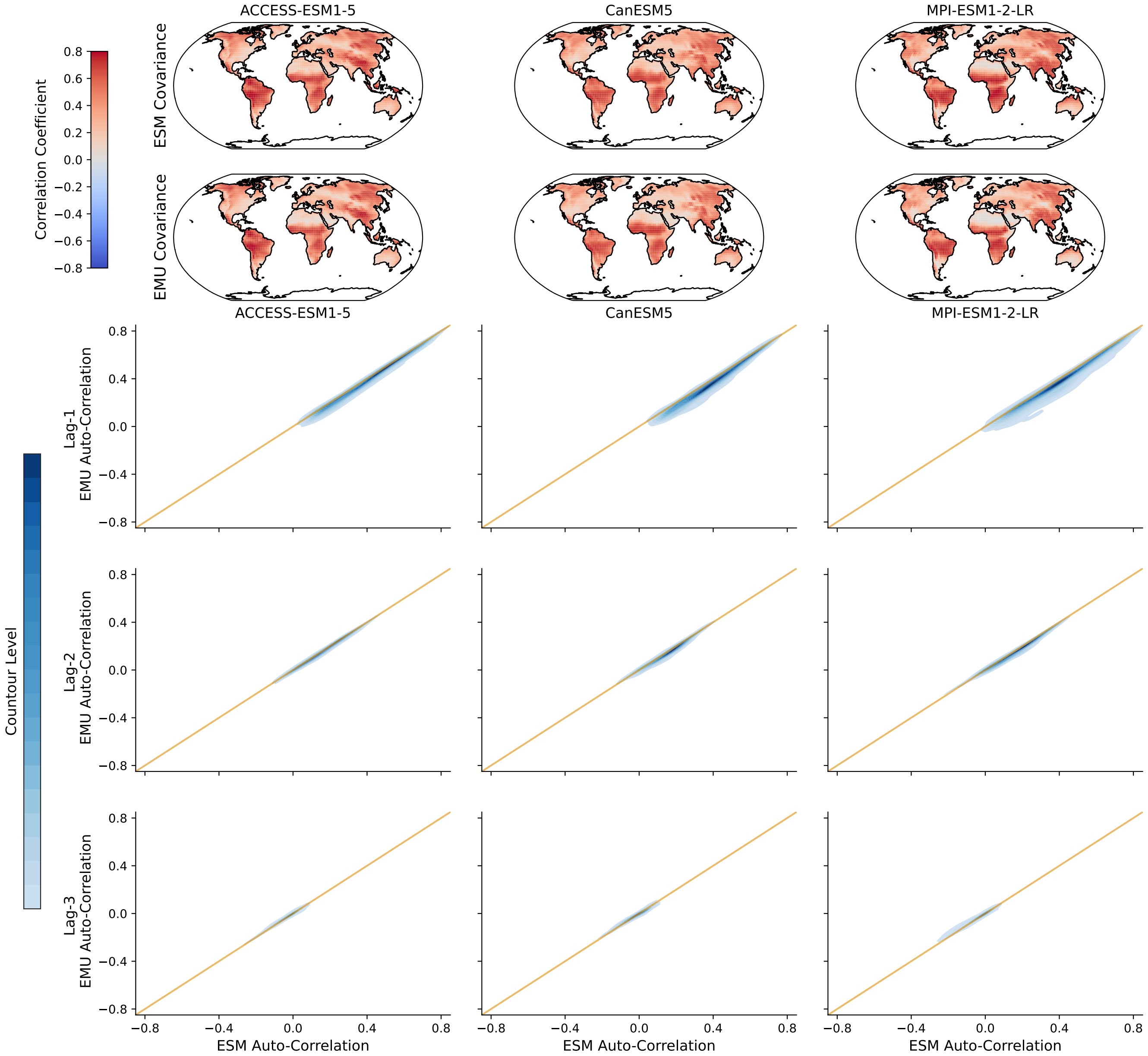

Figure 6. Lagged auto-correlations across grid-points for three different models (columns). Upper subfigure: Spatial distribution of lag-1 auto-autorrelations for ESM/ EMU data (upper/lower panel). Lower subfigure: Distribution of emulated auto-correlations (y-Axis) against ESM auto-correlations (x-Axis) for three different time lags (lag-1,lag-2 and lag-3 in the upper, middle and lower panel respectively). The orange line represents the ideal distribution (EMU estimates exactly equal ESM estimates). The distribution was obtained using a KDE estimate with contour levels from 5%-95% in 5% intervals, meaning every shade of blue represent 5% of all data points and an additional 5% lie outside the shaded area.

https://doi.org/10.5194/egusphere-2024-278
Preprint. Discussion started: 13 May 2024
© Author(s) 2024. CC BY 4.0 License.

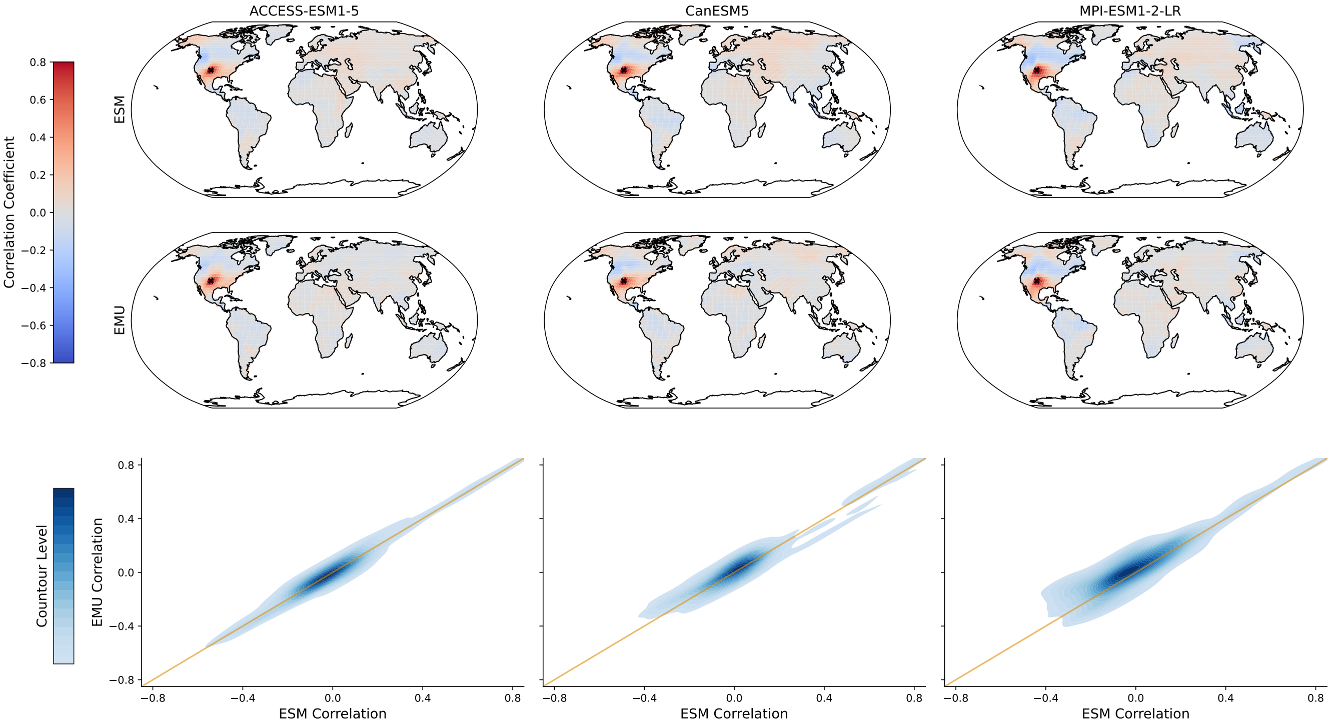

Figure 7. Spatial correlations between precipitation signals for January. Upper subfigure: Correlation between precipitation at a randomly chosen gridpoint (New Mexico with lat: 36.25, lon: -103.75; coloured in dark red as the correlation of a timeseries with itself is 1) and precipitation at all other gridpoints for three models (columns: ACCESS-ESM1-5, CanESM5, MPI-ESM1-2-lR) and for ESM (upper panel) and EMU data (lower panel). Lower subfigure: Correlations between any possible combination of precipitation timeseries (that is correlations between $Pr_{s,m=1}$ and $Pr_{r,m=1}$ for any possible combination of spatial locations (s, r)). EMU estimates (y-Axis) plotted against ESM estimates (x-Axis). The orange line represents the ideal distribution (EMU estimates exactly equal ESM estimates). The distribution was obtained using a KDE with contour levels from 5%-95% in 5% intervals, meaning every shade of blue represent 5% of all data points and an additional 5% lie outside the shaded area.

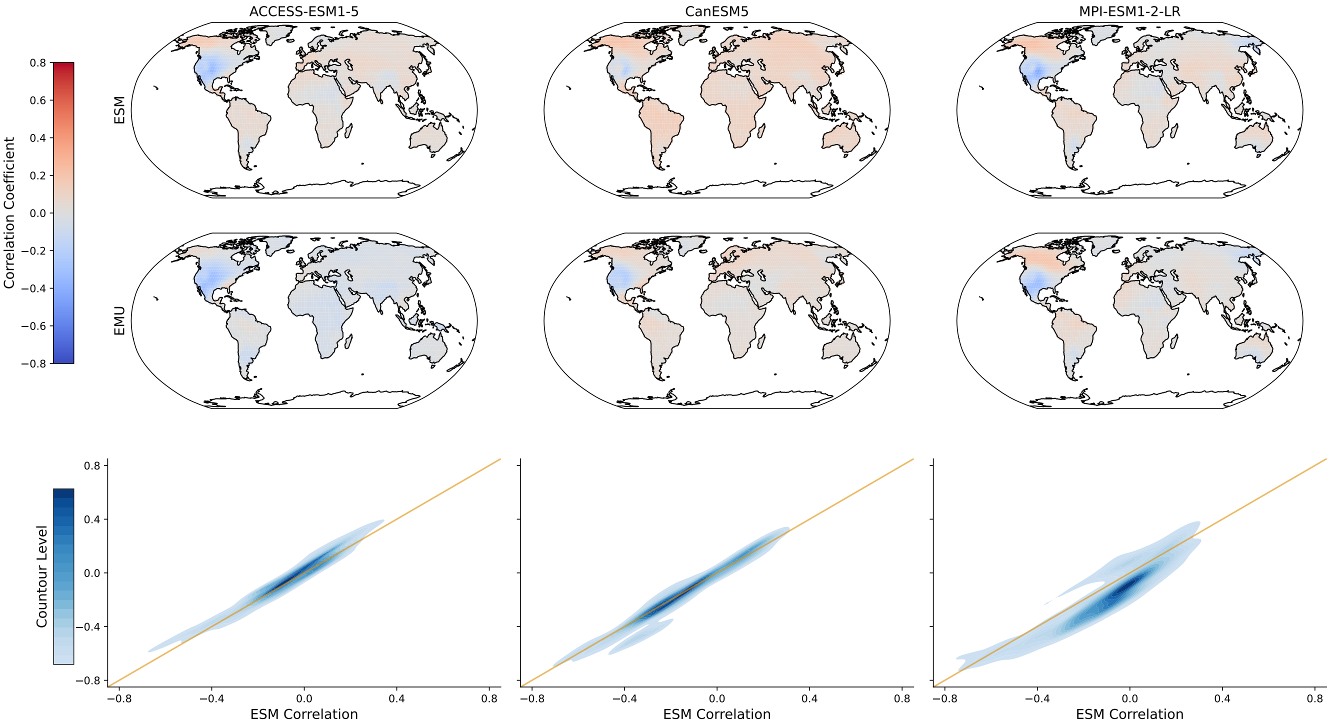

Figure 8. Spatial correlations between precipitation and temperature for January. Upper subfigure: Correlation between precipitation at a randomly chosen gridpoint (New Mexico with lat: 36.25, lon: -103.75) and temperature at all other gridpoints for three models (columns: ACCESS-ESM1-5, CanESM5, MPI-ESM1-2-lR) and for ESM (upper panel) and EMU data (lower panel). Lower subfigure: Correlations between any possible combination of precipitation and temperature timeseries (that is correlations between $Pr_{s_i,m=1}$ and $T_{s_j,m=1}$ for any possible combination of spatial locations $(s_i,\, s_j)$). EMU estimates (y-Axis) plotted against ESM estimates (x-Axis). The orange line represents the ideal distribution (EMU estimates exactly equal ESM estimates). The distribution was obtained using a KDE with contour levels from 5%-95% in 5% intervals, meaning every shade of blue represent 5% of all data points and an additional 5% lie outside the shaded area.

© Author(s) 2024. CC BY 4.0 License.

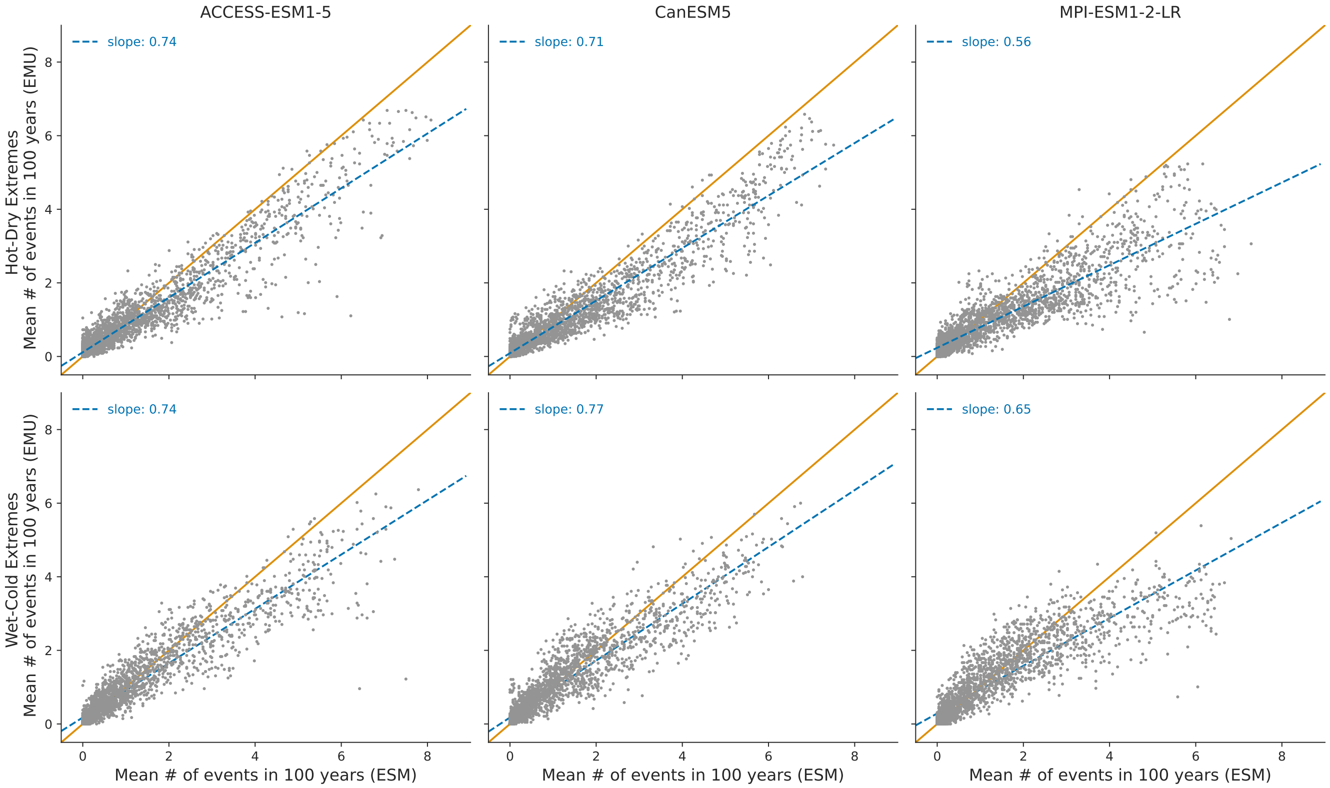

Figure 9. Distribution of compound temperature-precipitation extremes in January. Number of compound extreme events are estimated at each grid point (every dot represents one gridpoint) and counted as explained in Sect. 3.3. Number of compound extremes found in EMU (y-Axis) plotted against the number of events found in ESM data (x-Axis). Orange line represents the ideal distribution (number of events in EMU equals number of events in ESM).

Fig. B5); while CanESM5 projects fairly strong, positive long range correlations, MPI-ESM1-2-LR projects moderate negative correlations.

Figure 9 displays the distribution of compound temperature and precipitation extremes. Our framework is generally able to capture compound temperature-precipitation extremes, but typically underestimates them. In January, the strongest underestimations of both (hot-dry and cold-wet) extremes occur in Australia, Central and Southern Africa and at the North-Eastern parts of South America. In July, the strongest underestimations are present over the Sahel region, the Arabian Peninsula and the area adjacent to the Gulf of Mexico. The strength of the underestimation is comparable for January and July (see Fig. B7).

5 Discussion and Conlusion

We have developed and validated an Earth System Model (ESM) emulator that derives monthly, spatially explicit precipitation data from monthly, spatially explicit temperature data. We have shown that our framework captures temporal and spatial

https://doi.org/10.5194/egusphere-2024-278
Preprint. Discussion started: 13 May 2024
© Author(s) 2024. CC BY 4.0 License.

precipitation structures and produces realistic cross-variable correlation structures. More precisely, we validated inter-annual trend and variability characteristics along with month-to-month variability. The strongest deviations between the emulated and the ESM distributions occur in the tails of the precipitation distribution (mainly above the 95% quantile) where we could observe some slight (usually smaller than 10%) systematic over-estimations of ESM quantiles. This might imply that some of the assumptions underlying the emulation framework are not holding anymore in extreme cases.

Extreme precipitation events can be driven by different physical processes and variables. For example, in low latitudes very extreme precipitation events are often linked to the occurrence of tropical storms or cyclones (Khouakhi et al., 2017). The physical dynamics governing such singular events of strong convective precipitation are not resolved in our statistical approach. We aim at modelling precipitation across different temporal scales and different spatial locations relying on the same statistical model. This naturally comes with limitations. These limitations also become visible when jointly modelling temperature-precipitation extremes. Our framework is generally able to capture compound extremes and produces realistic spatial patterns. However, our emulator generally underestimates the occurrence of joint extremes. The emulator tends to slightly overestimate the magnitude of precipitation above the 95% quantile while simultaneously underestimating the occurrence rate of joint temperature-precipitation extremes, which suggests that the assumption of the precipitation residuals being independent of temperature is likely not fully accurate. In reality, the residuals are likely still not fully stationary and either depend on global or local temperature and potentially also the predictions from the temperature-driven precipitation response. In addition, the emergence of compound extremes may depend on additional feedback effects, for example soil-moisture in the case of heat-drought events (Jha et al., 2023). It is noteworthy, however, that the deviations of the emulated results from the actual ESM results are much smaller than inter-ESM differences.

In a next step, we have forced our precipitation emulator with emulated temperatures (see Appendix C1). The performance is comparable to the results obtained using ESM data as forcing (spee Appendix C2).

There are multiple ways in which our approach could be further refined and adapted to different tasks. For once, instead of solely relying on Gamma GLMs thereby imposing a fixed mean-variance relationships at each location, the approach could be adjusted to optimise for other distribution families. In addition, the validation approach could be extended to other SSP scenarios. Specifically to scenarios that do not show continuous warming as transient and quasi-equilibrium climate states have been show to have substantial local differences (King et al., 2021). To correctly model overshoot scenarios, it will also be necessary to include additional predictors. While local temperatures over land to some extent follow GMT under a reversal of the global mean temperature trend, changes in regional precipitation are not expected to be reversed in the short term in many regions (Pfleiderer et al., 2023). Beusch et al. (2022) have made some efforts to overcome these difficulties by including ocean heat uptake as an additional predictive variable for local temperatures. Similar efforts could be pursued for precipitation. Lastly, the modelling framework could be improved by adjusting the residual variability module to account for a link between the predicted mean response and the distribution of additional variability. This would allow for non-stationary relationships in the variability module and overcome some limitations in the tails of the distribution.

To conclude, we offer a robust emulation framework for modelling spatially resolved, monthly precipitation from spatially resolved, monthly temperatures. In particular, the emulated precipitation field is spatially and temporally consistent with the

© Author(s) 2024. CC BY 4.0 License.

temperature data used as forcing. Our emulation framework offers exciting new opportunities and is a step towards making climate science more accessible. While ESMs are costly and data intensive to run, Open Source emulators are available to everyone for projecting regional climate impacts. This is particularly important as temperature and precipitation extremes are among the most impactful consequences of climate change. In addition, the emulator provides numerous applications, for example, coupling to impact models to provide an efficient modelling chain for translating emission scenarios directly into climate impacts. A promising avenue for this could be to couple our emulator to an emulator offering agricultural variables (e.g., Abramoff et al., 2022).

Code and data availability. The current version of the model MESMER-M-TP is available on GitHub: https://github.com/sarasita/mesmer-m-tp. The exact version of the model used to produce the results used in this paper is archived on Zenodo (https://zenodo.org/doi/10.5281/zenodo.11086167, Schöongart, 2024). In addition, code for MESMER and MESMER-M can be found at https://github.com/MESMER-group/mesmer. Whenever MESMER(-M) data was used in this study, we relied on MESMER v0.9.0 available on Zenodo (https://doi.org/10.5281/zenodo.10408206, Hauser et al., 2023). The analysis can be reproduced using the code on Zenodo and ESM data as described in Brunner et al. (2020) available from the public CMIP archive at https://esgf-node.llnl.gov/projects/cmip6/.

Appendix A: Earth System Model Data

Table A1. Overview of the 24 ESMs that are part of this study and the scenarios that are available for each model. The number of realisations counts only ensemble members that have data for all indicated scenarios. The training run column contains the identifier of the run that is used for training. All available runs except the training run are used for testing. If no testing run is available, we include the training run. The three models with the largest number of available runs are highlighted and play a special role for evaluating the emulator performance.

Model name	Reference	Available scenarios	# of realisations	Training run
ACCESS-CM2	Dix et al. (2019)	SSP1-2.6, SPP2-4.5, SPP3-7.0, SPP5-8.5	5	r1i1p1f1
ACCESS-ESM1-5	Ziehn et al. (2019)	SSP1-2.6, SPP2-4.5, SPP3-7.0, SPP5-8.5	**40**	r1i1p1f1
AWI-CM-1-1-MR	Semmler et al. (2019)	SSP1-2.6, SPP2-4.5, SPP3-7.0, SPP5-8.5	1	r1i1p1f1
CESM2-WACCM	Danabasoglu (2019b)	SSP1-2.6, SPP2-4.5, SPP3-7.0, SPP5-8.5	3	r1i1p1f1
CESM2	Danabasoglu (2019a)	SSP1-2.6, SPP2-4.5, SPP3-7.0, SPP5-8.5	1	r1i1p1f1
CMCC-CM2-SR5	Lovato and Peano (2020)	SSP1-2.6, SPP2-4.5, SPP3-7.0, SPP5-8.5	1	r1i1p1f1
CNRM-CM6-1-HR	Voldoire (2019b)	SSP1-2.6, SPP2-4.5, SPP3-7.0, SPP5-8.5	1	r1i1p1f2
CNRM-CM6-1	Voldoire (2019a)	SSP1-2.6, SPP2-4.5, SPP3-7.0, SPP5-8.5	6	r1i1p1f2
CNRM-ESM2-1	Seferian (2019)	SSP1-1.9, SSP1-2.6, SPP2-4.5, SPP3-7.0, SPP5-8.5	5	r1i1p1f1
CanESM5	Swart et al. (2019)	SSP1-1.9, SSP1-2.6, SPP2-4.5, SPP3-7.0, SPP5-8.5	**50**	r1i1p1f1
E3SM-1-1	Bader et al. (2020)	SPP5-8.5	1	r1i1p1f1
FGOALS-f3-L	YU (2019)	SSP1-2.6, SPP2-4.5, SPP3-7.0, SPP5-8.5	1	r1i1p1f1
FGOALS-g3	Li (2019)	SSP1-1.9, SSP1-2.6, SPP2-4.5, SPP3-7.0, SPP5-8.5	4	r1i1p1f1
FIO-ESM-2-0	Song et al. (2019)	SSP1-2.6, SPP2-4.5, SPP3-7.0, SPP5-8.5	3	r1i1p1f1
HadGEM3-GC31-LL	Good (2019)	SSP1-2.6, SPP2-4.5, SPP3-7.0, SPP5-8.5	4	r1i1p1f3
HadGEM3-GC31-MM	Jackson (2020)	SSP1-2.6, SPP5-8.5	4	r1i1p1f3
IPSL-CM6A-LR	Boucher et al. (2019)	SSP1-1.9, SSP1-2.6, SPP2-4.5, SPP3-7.0, SPP5-8.5	7	r1i1p1f1
MPI-ESM1-2-HR	Schupfner et al. (2019)	SSP1-2.6, SPP2-4.5, SPP3-7.0, SPP5-8.5	2	r1i1p1f1
MPI-ESM1-2-LR	Schupfner et al. (2021)	SSP1-1.9, SSP1-2.6, SPP2-4.5, SPP3-7.0, SPP5-8.5	**30**	r1i1p1f1
MRI-ESM2-0	Yukimoto et al. (2019)	SSP1-1.9, SSP1-2.6, SPP2-4.5, SPP3-7.0, SPP5-8.5	6	r1i1p1f1
NESM3	Cao (2019)	SSP1-2.6, SPP2-4.5, SPP5-8.5	2	r1i1p1f1
NorESM2-LM	Seland et al. (2019)	SSP1-2.6, SPP2-4.5, SPP3-7.0, SPP5-8.5	1	r1i1p1f1
NorESM2-MM	Bentsen et al. (2019)	SSP1-2.6, SPP2-4.5, SPP3-7.0, SPP5-8.5	1	r1i1p1f1
UKESM1-0-LL	Good et al. (2019)	SSP1-2.6, SPP2-4.5, SPP3-7.0, SPP5-8.5	5	r1i1p1f2

© Author(s) 2024. CC BY 4.0 License.

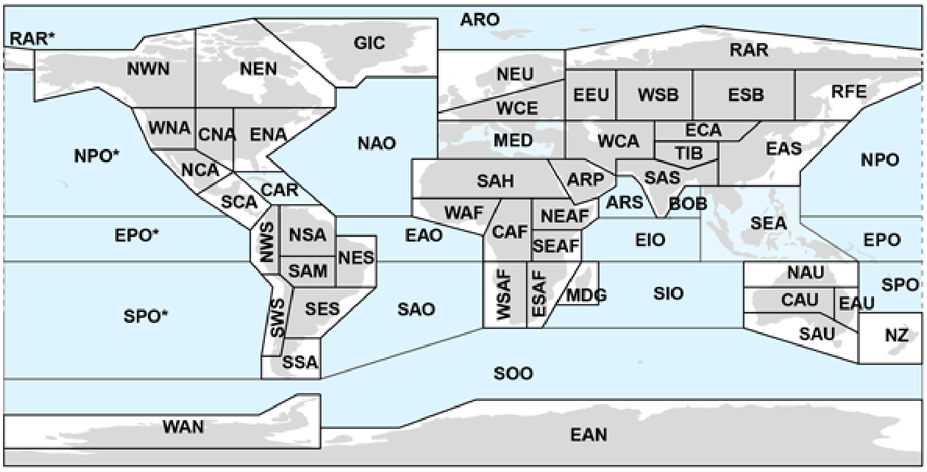

Figure A1. Map of all SREX regions including the 44 regions over land. From Iturbide et al. (2020).

395 Appendix B: Validation July

This section includes all graphics that were displayed for the direct emulation error in Sect. 4, but for July.

https://doi.org/10.5194/egusphere-2024-278
Preprint. Discussion started: 13 May 2024
© Author(s) 2024. CC BY 4.0 License.

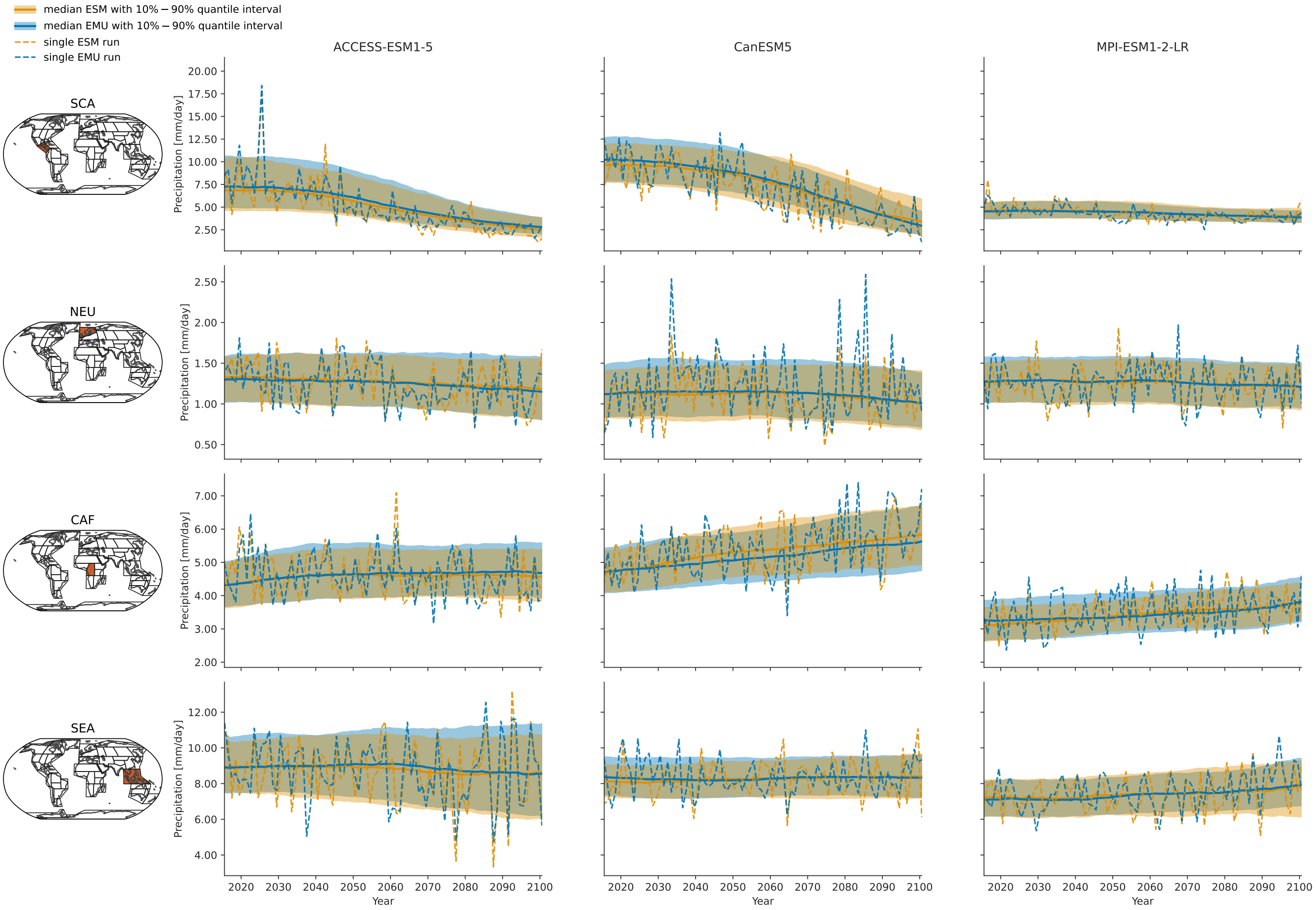

Figure B1. Same as Fig. 2 but for July.

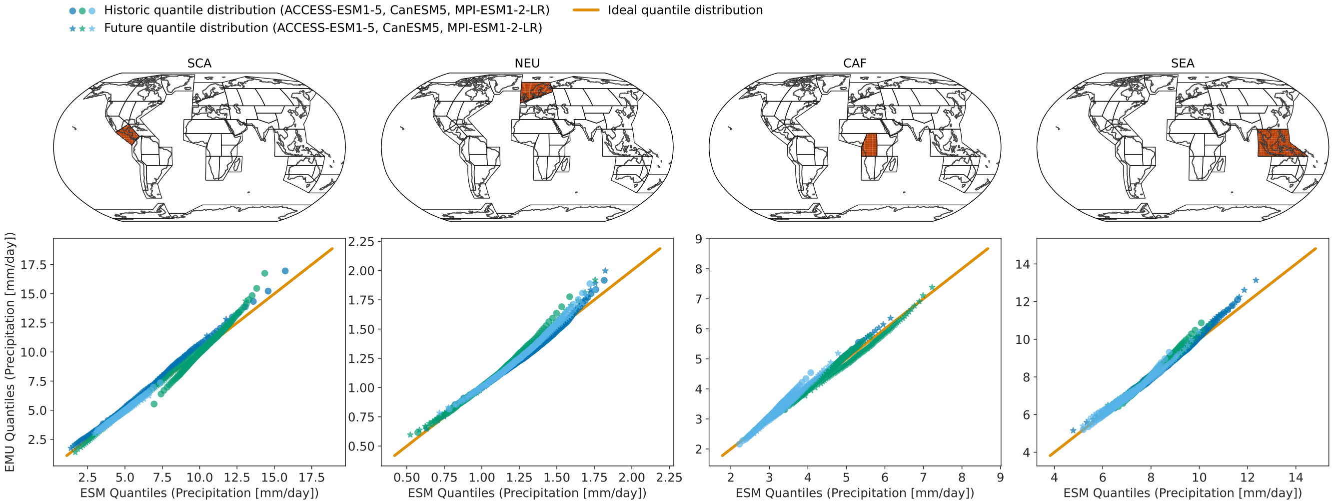

Figure B2. Same as Fig. 3 but for July.

https://doi.org/10.5194/egusphere-2024-278
Preprint. Discussion started: 13 May 2024
© Author(s) 2024. CC BY 4.0 License.

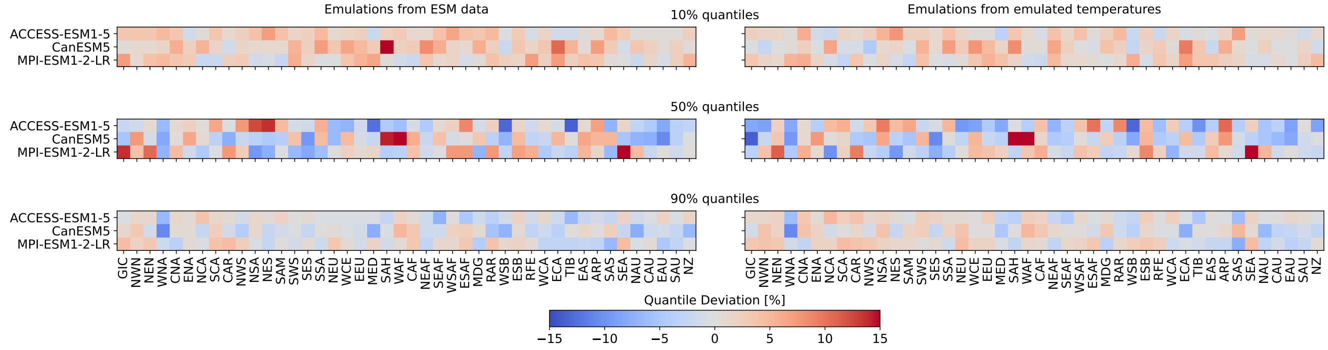

Figure B3. Same as Fig. 4 but for July.

© Author(s) 2024. CC BY 4.0 License.

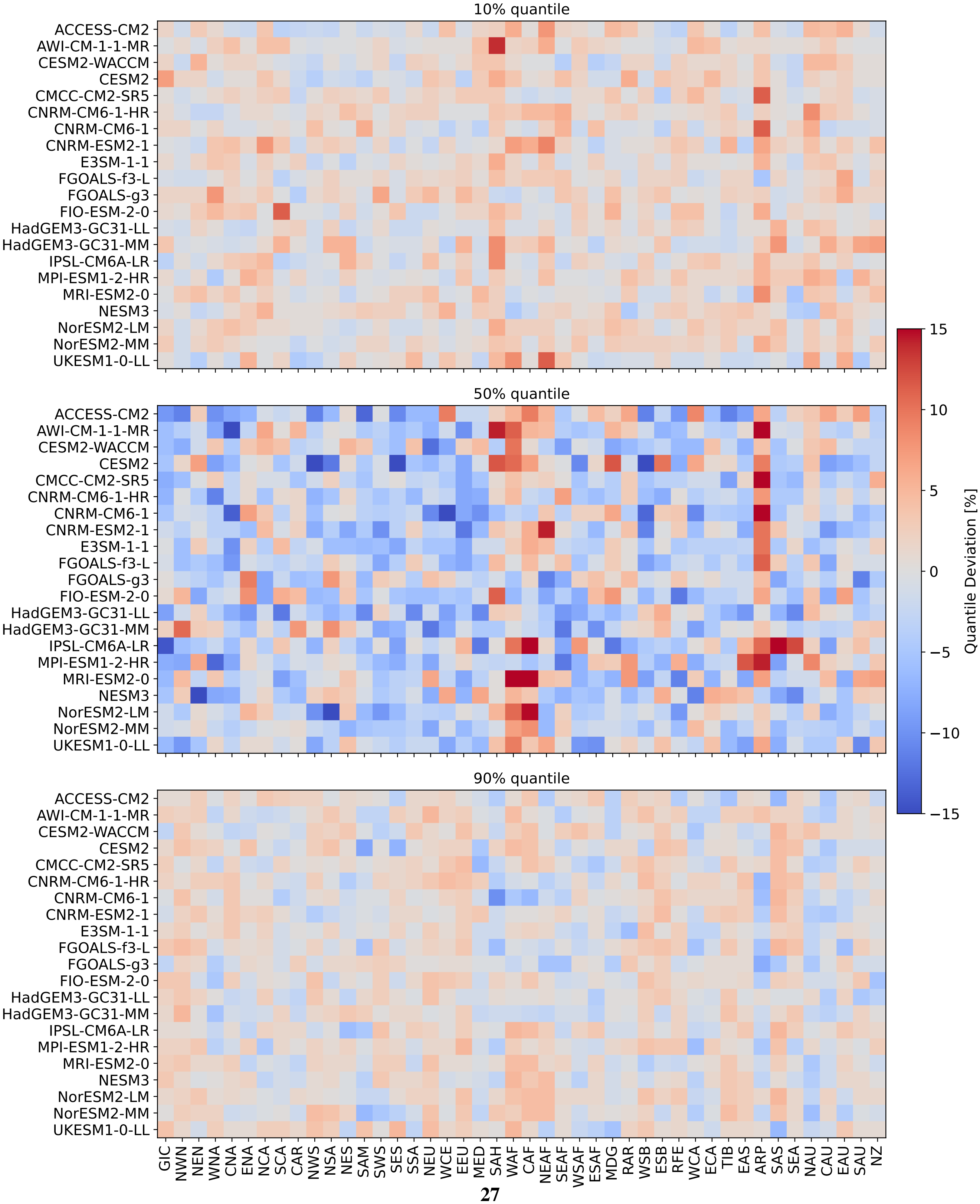

Figure B4. Same as Fig. 5 but for July.

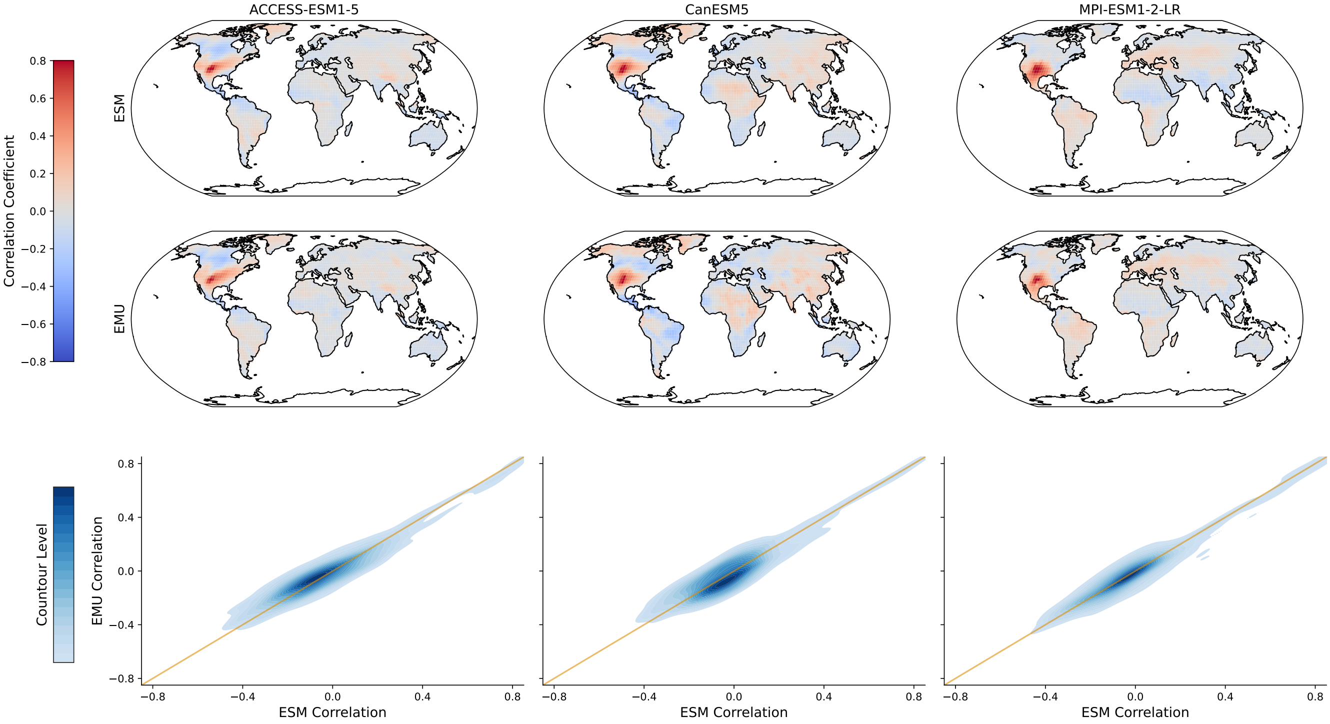

Figure B5. Same as Fig. 7 but for July.

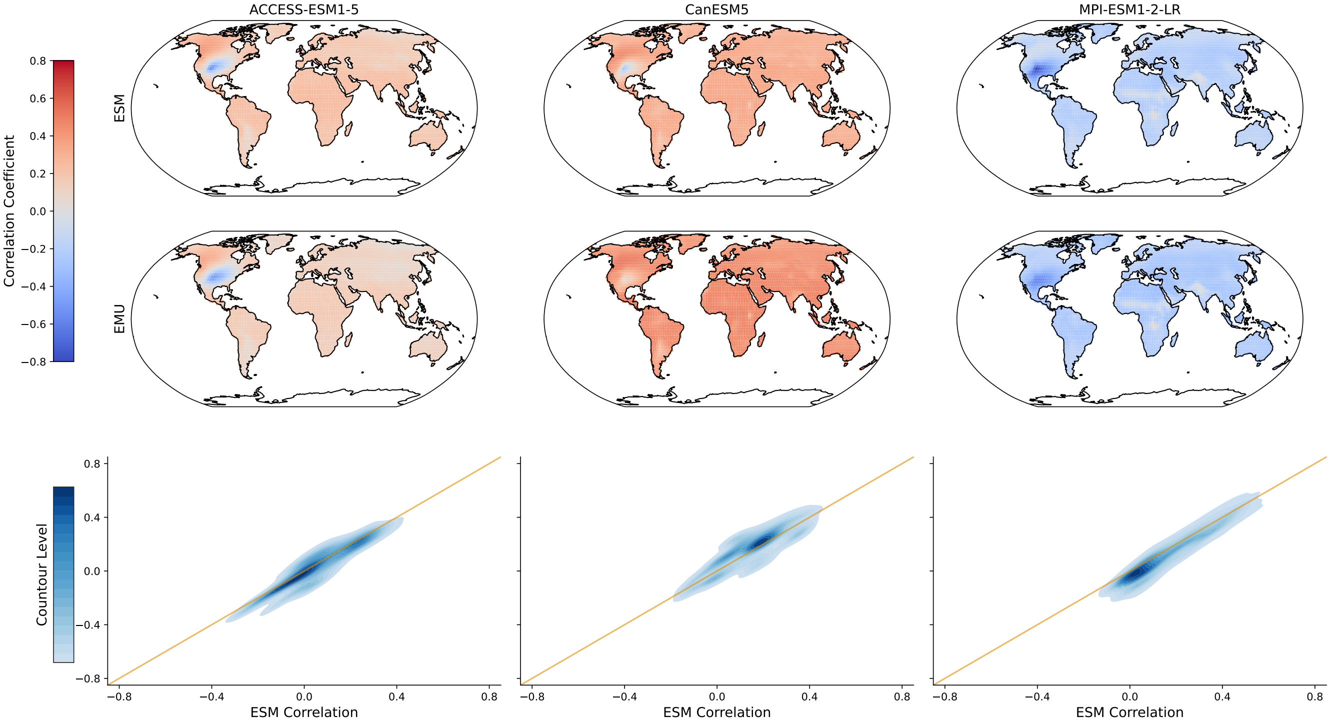

Figure B6. Sane as Fig. 8 but for July.

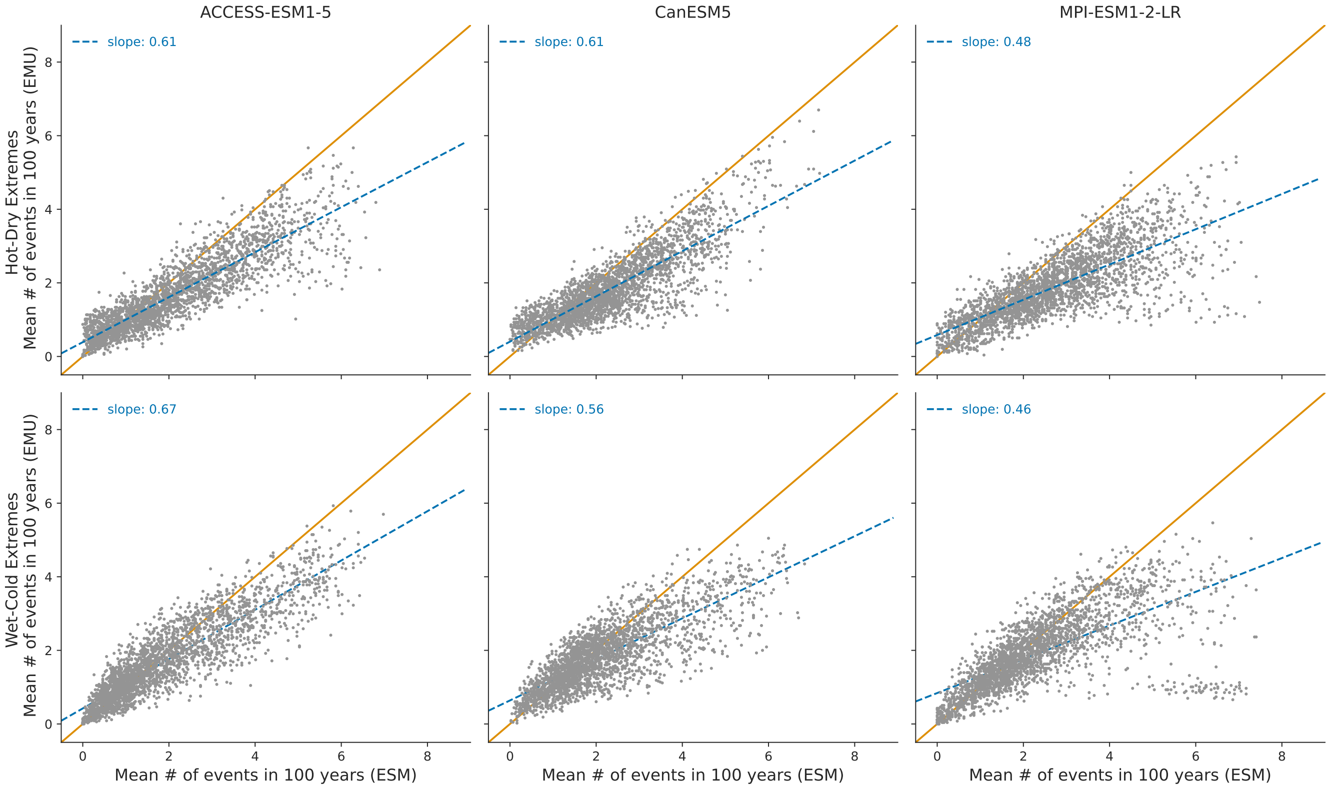

Figure B7. Same as Fig. 9 but for July.

Appendix C: Forcing MESMER-M-TP with Emulated Temperatures

C1 Generating a Dataset of Emulated Temperatures

We have generated simplified temperature emulations solely for assessing the quality of emulated precipitation data when our modelling framework is employed in a chain of computationally efficient emulators. The temperature emulations are only meant as a proof-of-concept to demonstrate the robustness of the approach to forcing data. Temperature emulations were generated as follows. First, the temperature field was projected onto its principal components (PCs). Next, a linear model was fitted to each principal component individually with the trend and the variability in global mean temperature (GMT) as the two sole predictive variables. GMT was decomposed into a trend and a variability component as suggested in Beusch et al. (2020). We then computed the residuals as the difference between the original principal components and the linear fit. Next, we used a Yeo-Johnson transform to ensure the residuals follow a normal distribution. Subsequently, we approximated the residuals as an Auto-Regressive (AR) process of order 1 as suggested in Nath et al. (2022). In order to generate temperature emulations, we generated additional realisations of GMT as described in Beusch et al. (2020) and used the regression coefficient to get

© Author(s) 2024. CC BY 4.0 License.

different realisations of the trend in the PCs. Then, we drew new samples from the AR(1) process and employed the inverse power transform to emulate variability. Lastly, we added the trend estimate and the variability samples and applied the inverse of the PCA to get a set of emulated temperatures. This way, we generated 100 temperature emulations for each model. In Fig. C1 and C2 we exemplary show timeseries of emulated temperature data and actual ESM temperature. An indication for the quality of the emulations are the quantile deviations shown in Fig. C3 and C4. The emulation approach usually works well, but is slightly underdispersive. In any case, we are only interested in the emulated temperature data to establish a proof of concept which is feasible with the presented emulation framework.

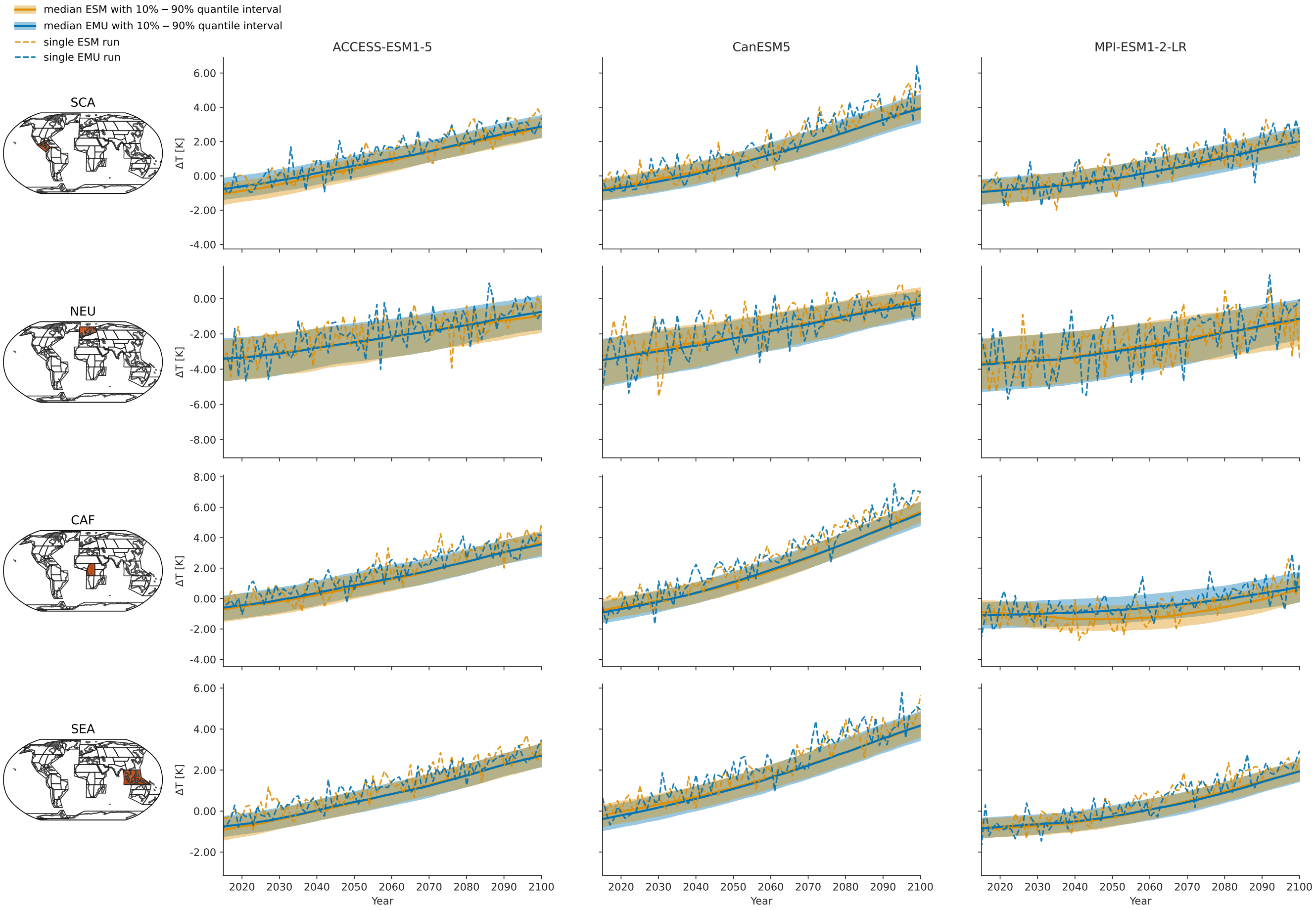

Figure C1. Same as Fig. 2 but for temperatures in January.

https://doi.org/10.5194/egusphere-2024-278
Preprint. Discussion started: 13 May 2024
© Author(s) 2024. CC BY 4.0 License.

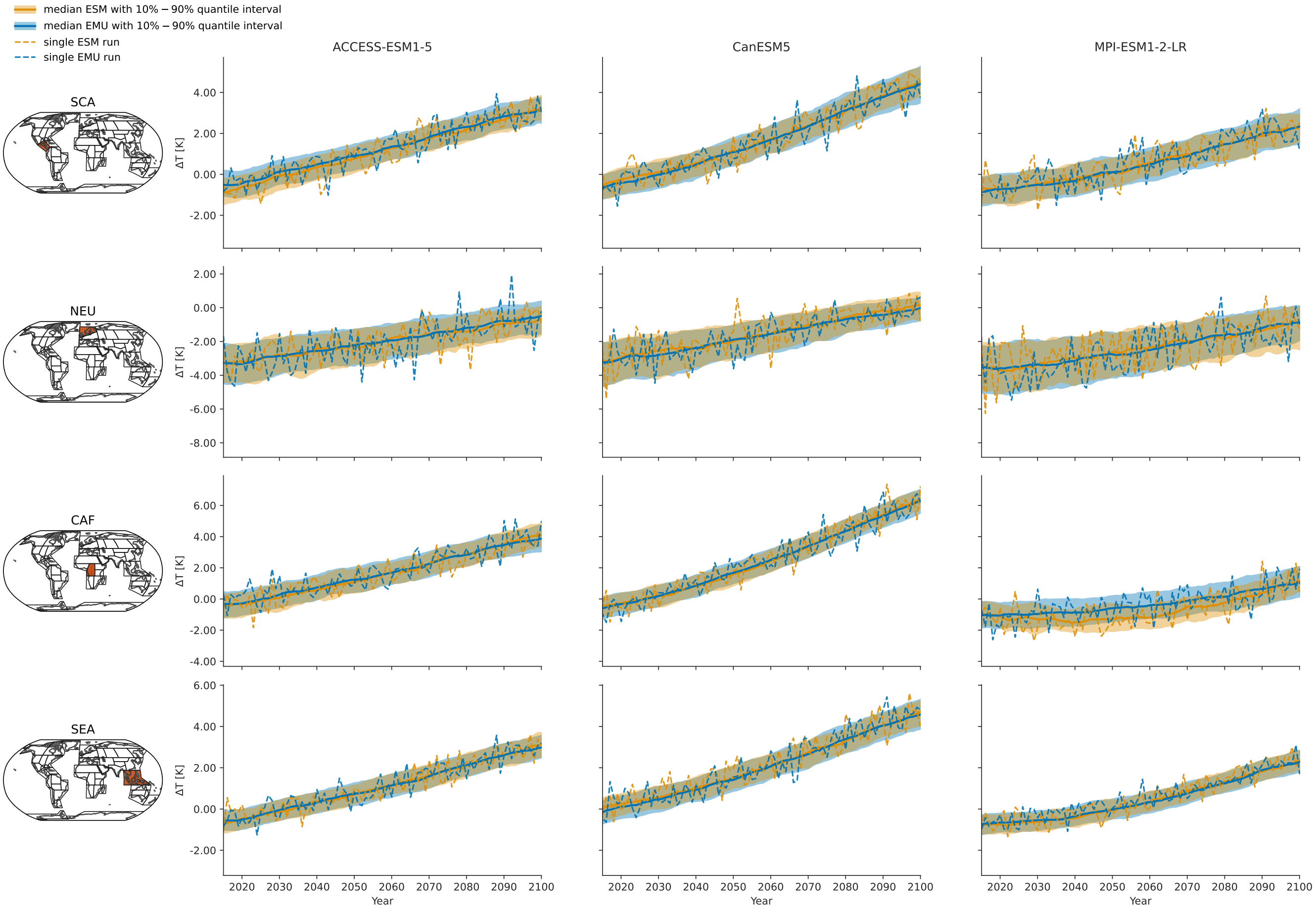

Figure C2. Same as Fig. 2 but for temperatures in July.

https://doi.org/10.5194/egusphere-2024-278
Preprint. Discussion started: 13 May 2024
© Author(s) 2024. CC BY 4.0 License.

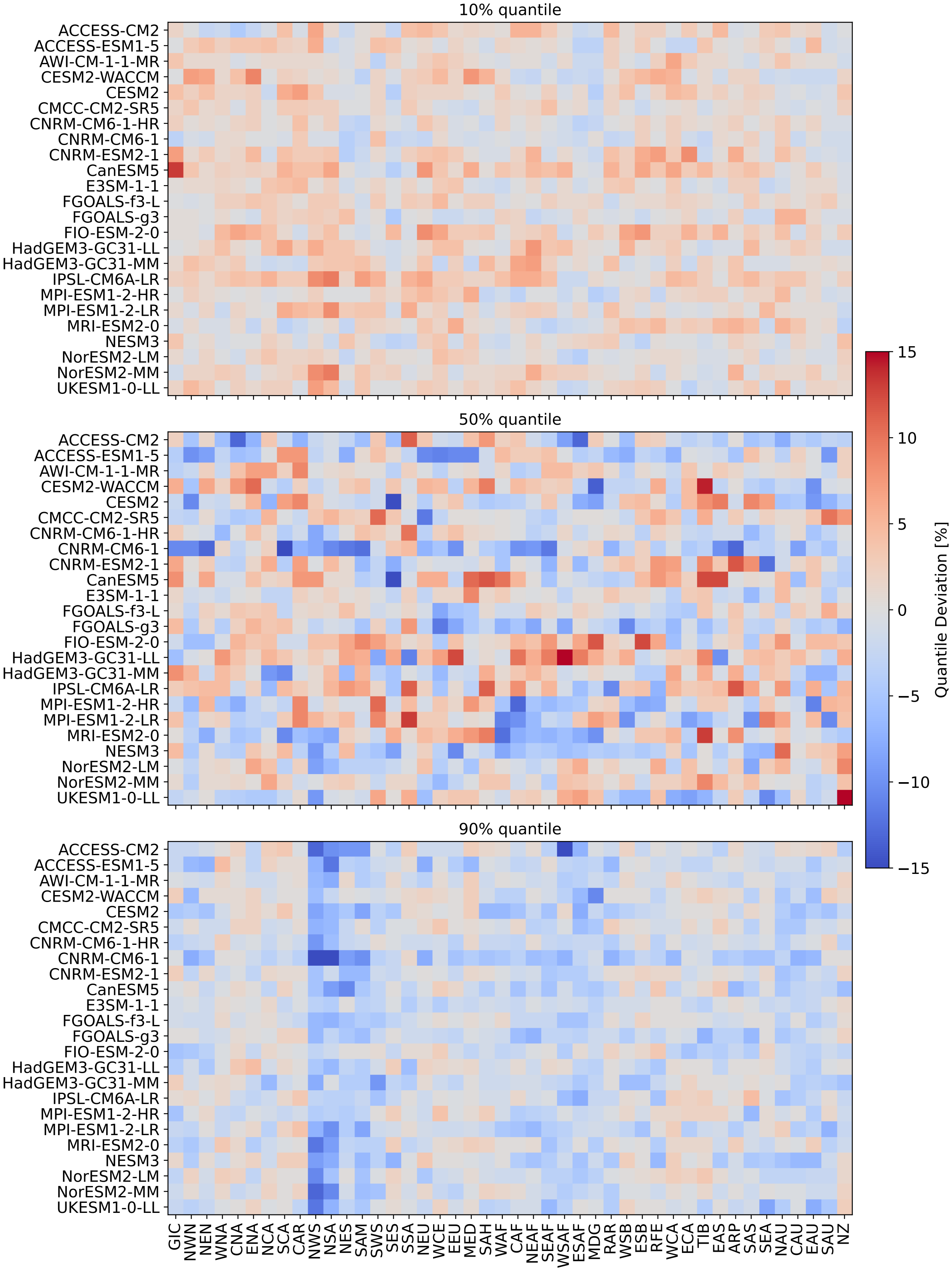

Figure C3. Same as Fig. 5 but for temperatures in January across all 24 models.

© Author(s) 2024. CC BY 4.0 License.

C2 Results for Coupled Emulations

This section presents all results shown in the main paper as well as in B for the coupled results.

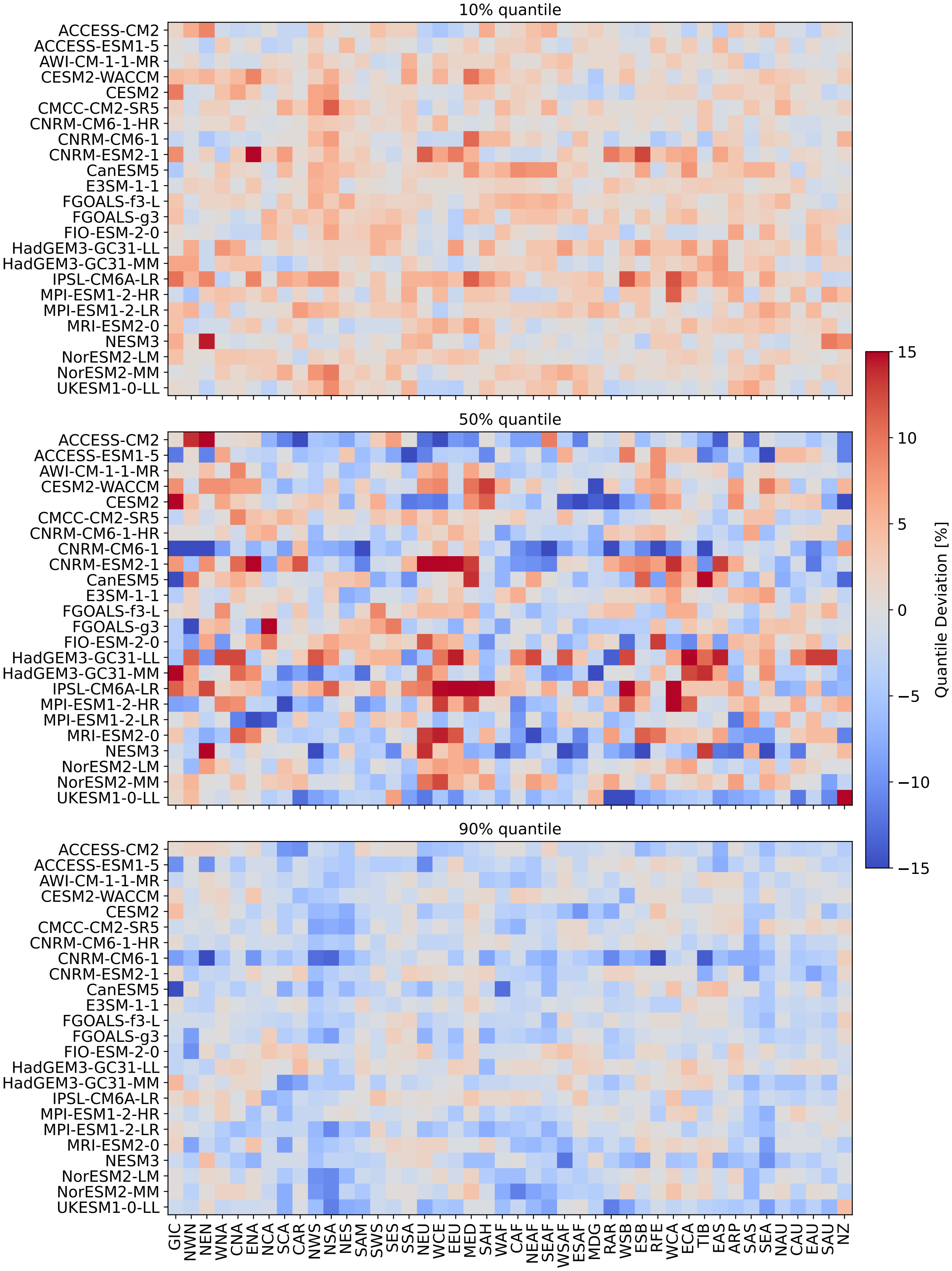

Figure C4. Same as Fig. 5 but for temperatures in July across all 24 models.

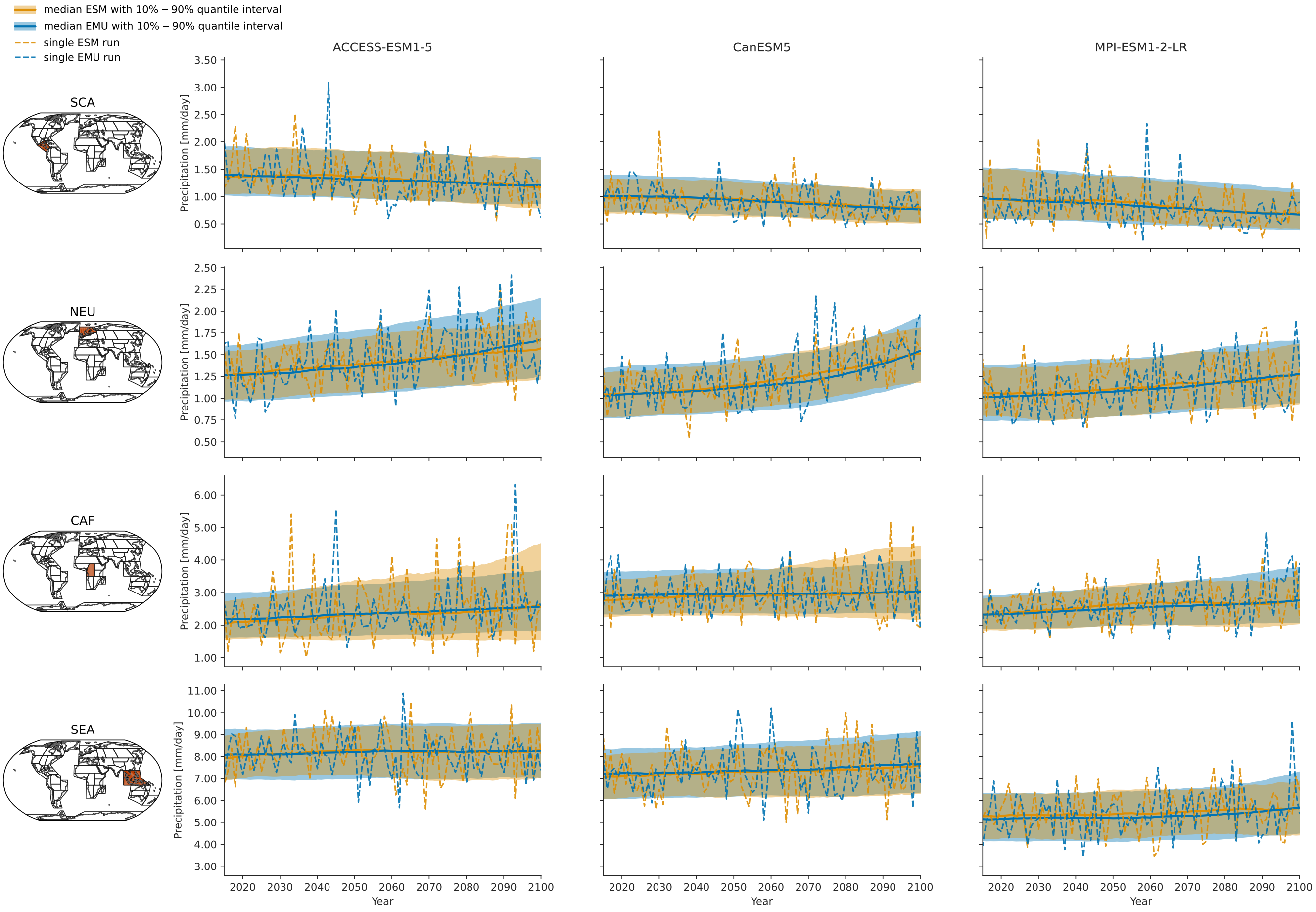

Figure C5. ame as Fig. 2 but for the coupled emulations in January.

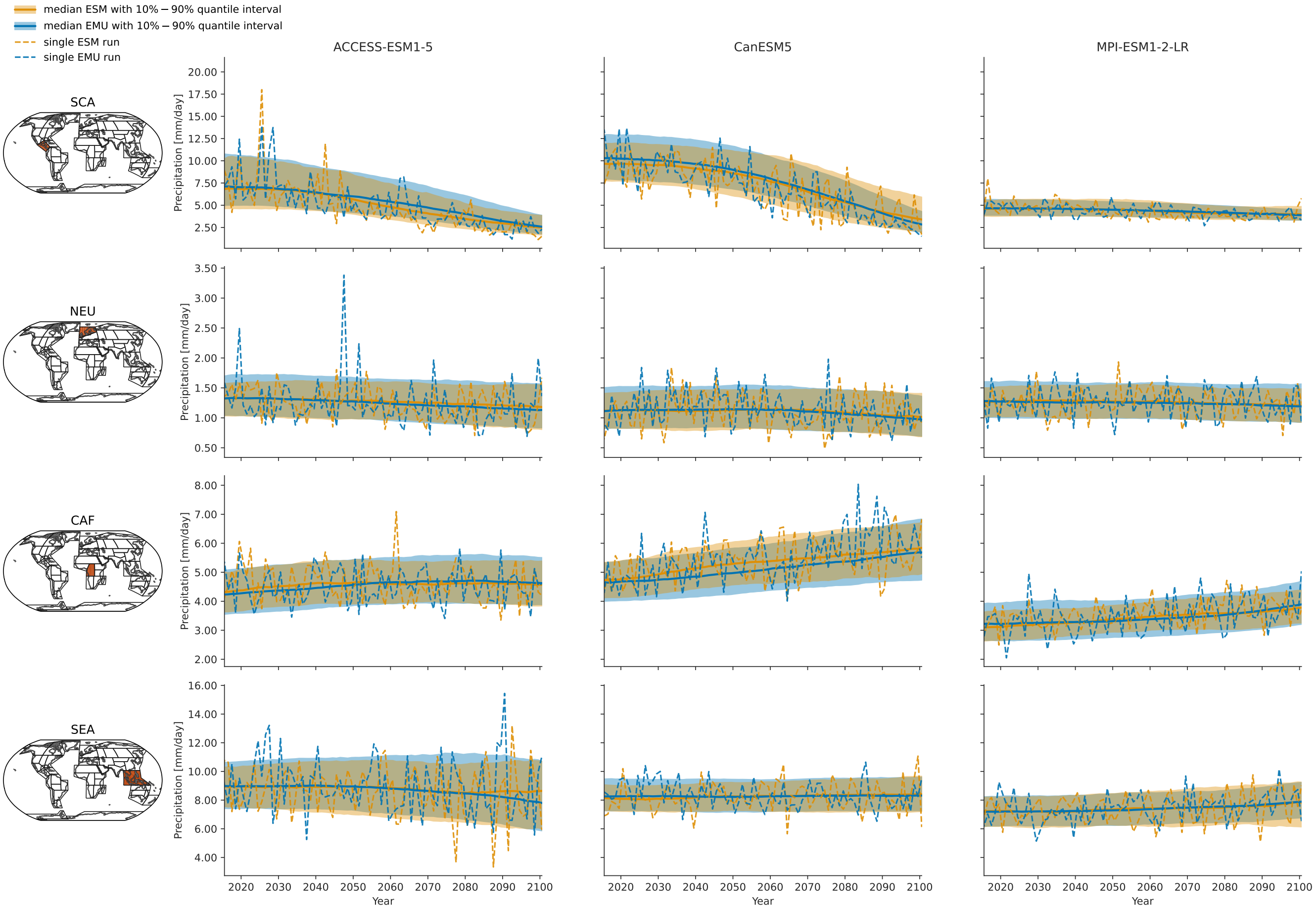

Figure C6. Same as Fig. 2 but for the coupled emulations in July.

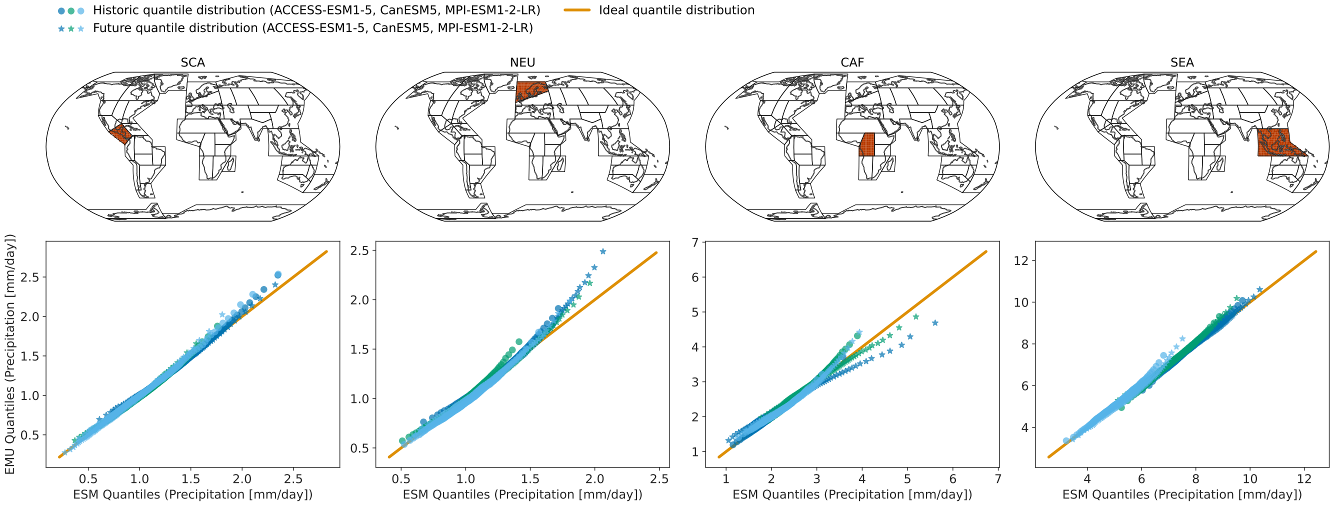

Figure C7. Same as Fig. 3 but for the coupled emulations in January.

https://doi.org/10.5194/egusphere-2024-278
Preprint. Discussion started: 13 May 2024
© Author(s) 2024. CC BY 4.0 License.

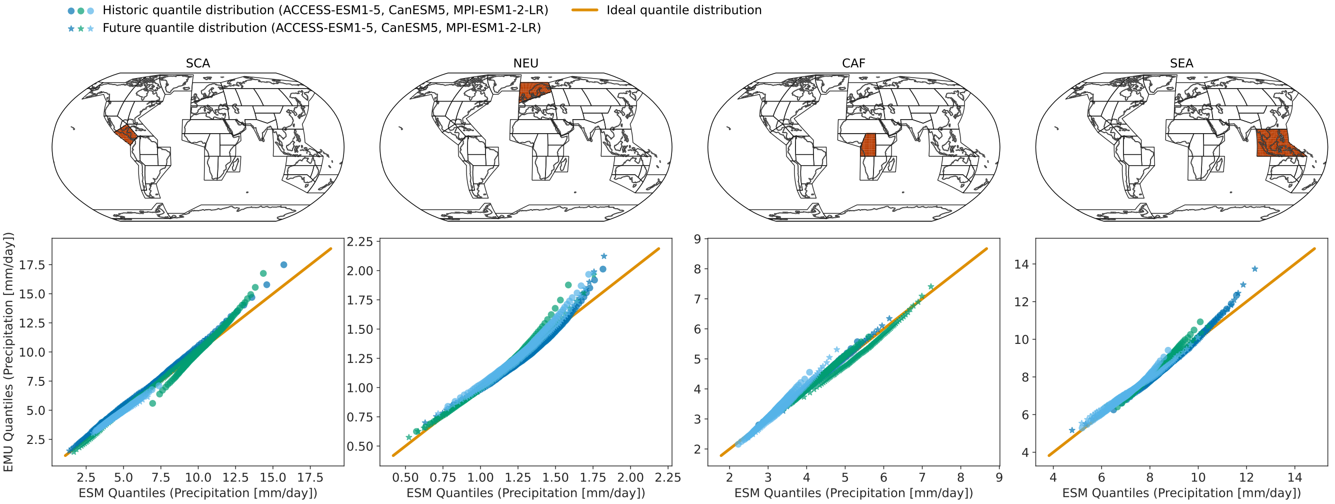

Figure C8. Same as Fig. 3 but for the coupled emulations in July.

© Author(s) 2024. CC BY 4.0 License.

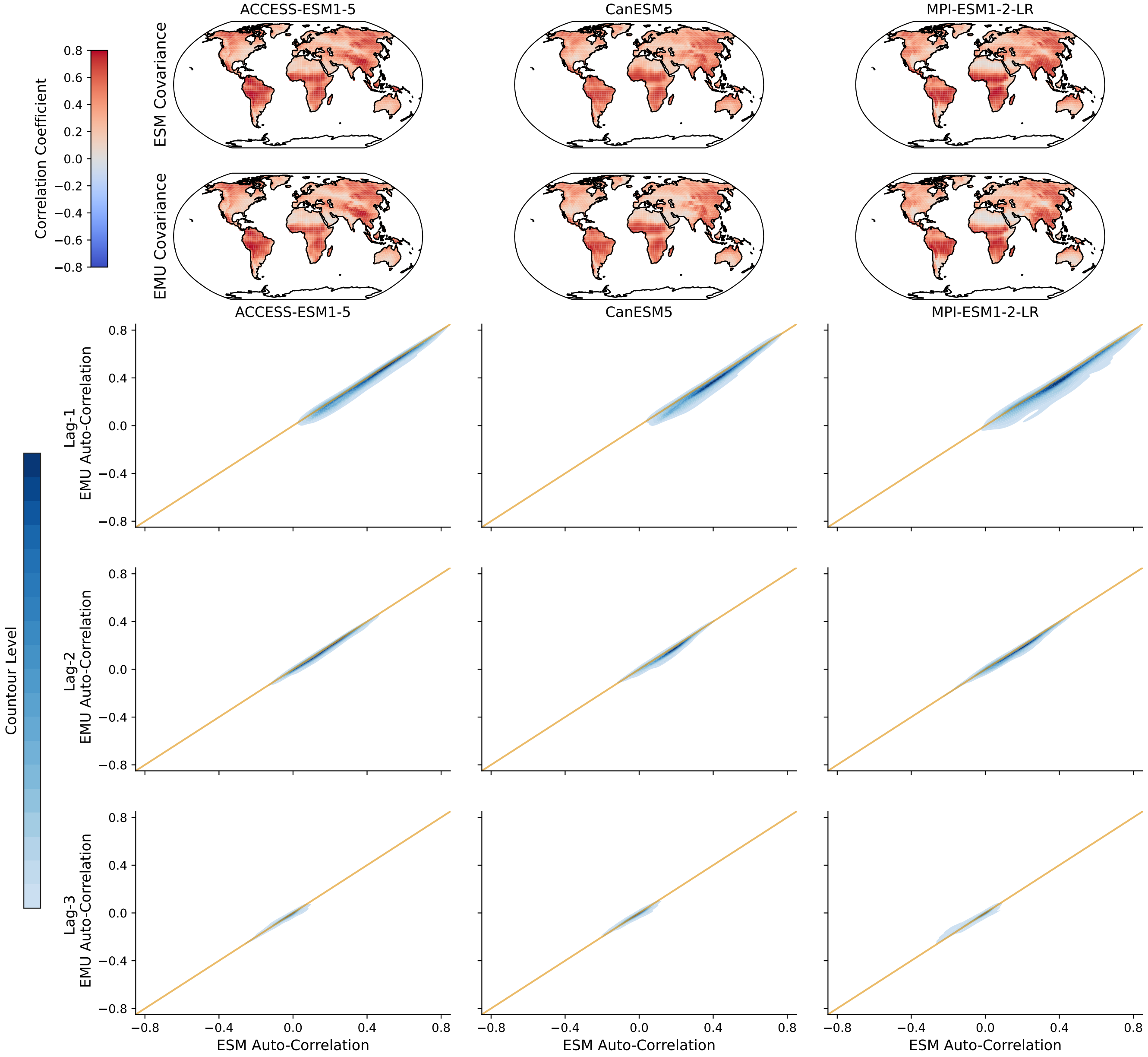

Figure C9. Same as Fig. 8 but for the coupled emulations in January.

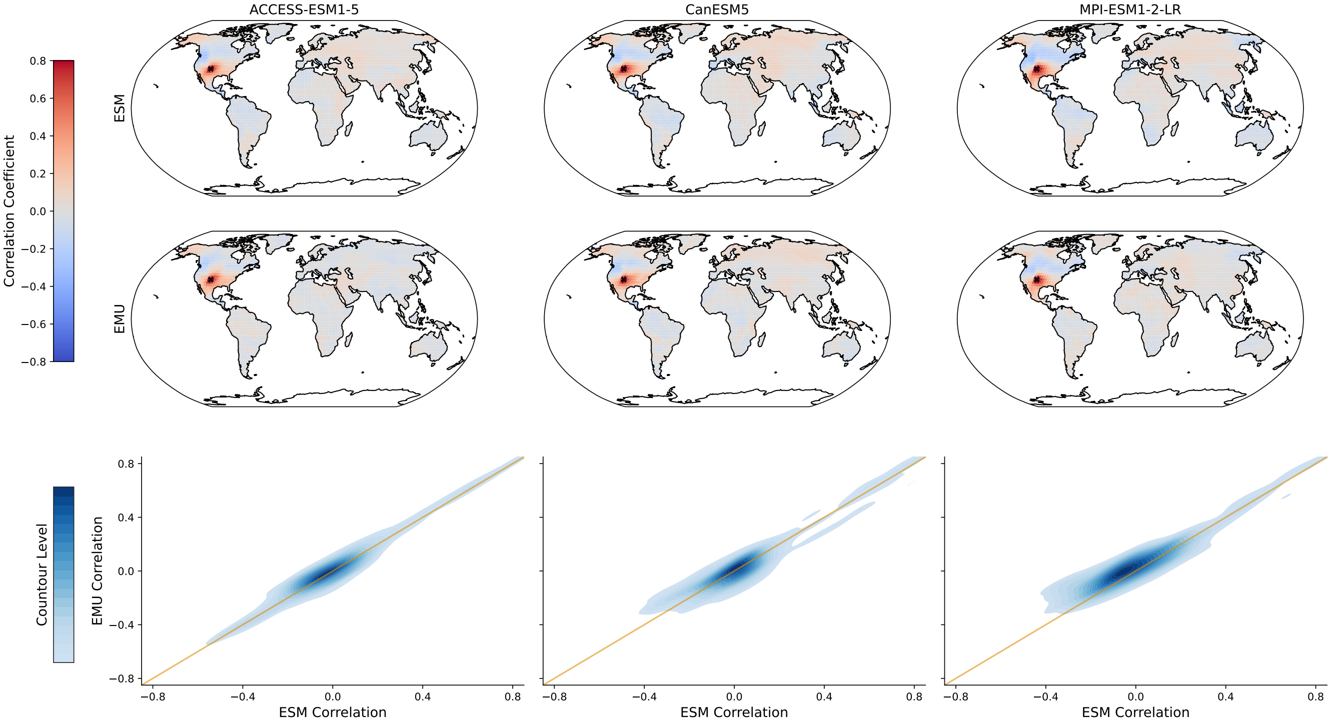

Figure C10. Same as Fig. 8 but for the coupled emulations in July.

© Author(s) 2024. CC BY 4.0 License.

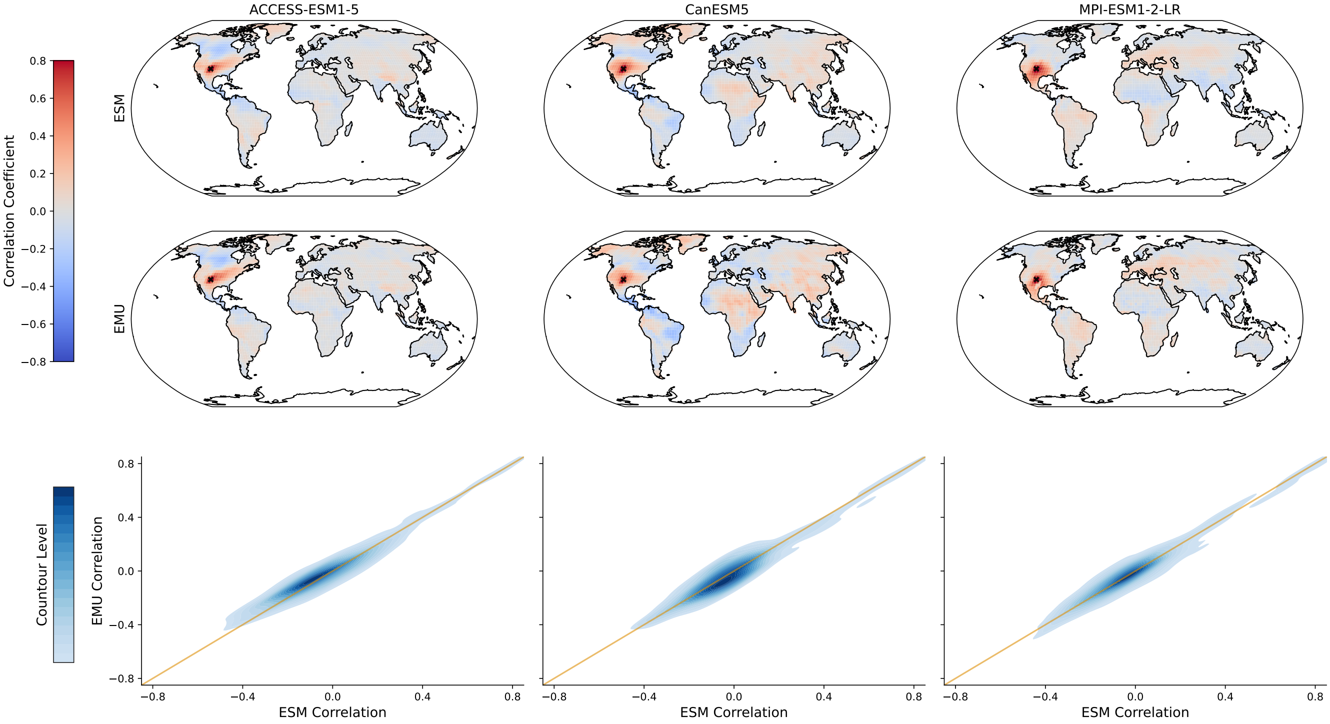

Figure C11. Same as Fig. 6 but for the coupled emulations

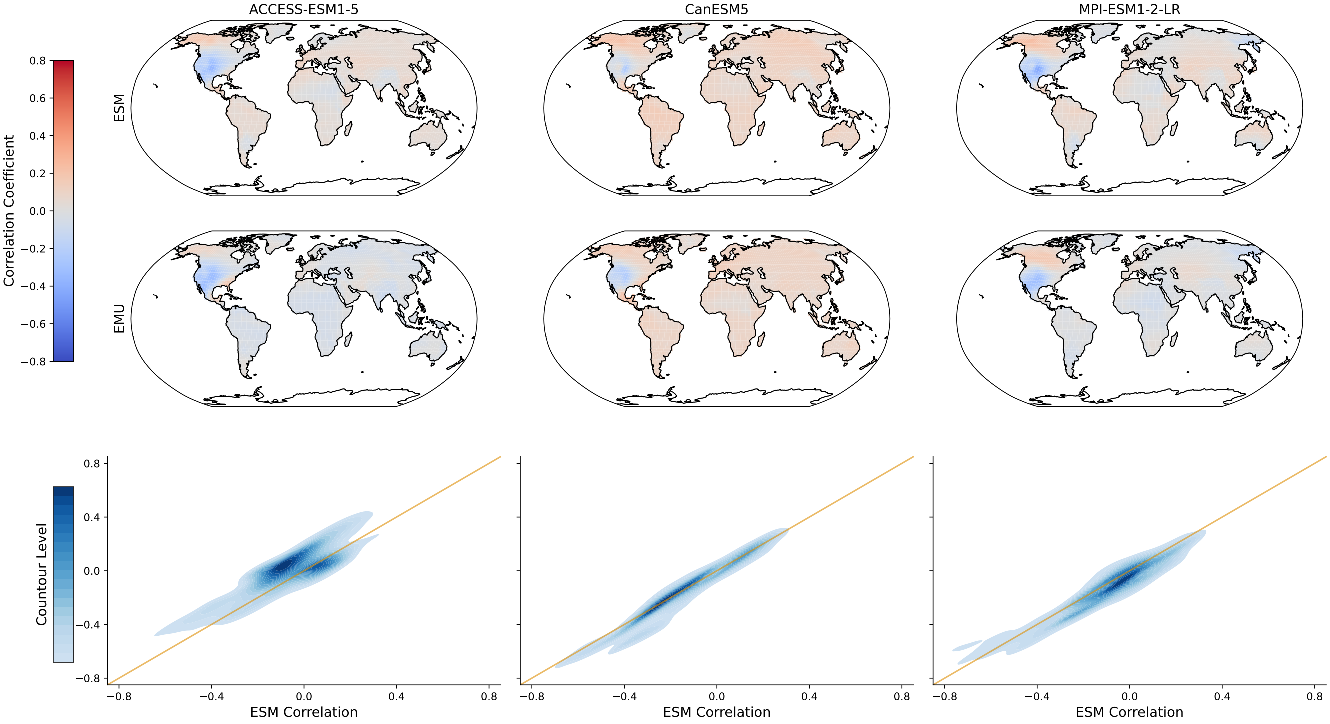

Figure C12. Same as Fig. 7 but for the coupled emulations in January.

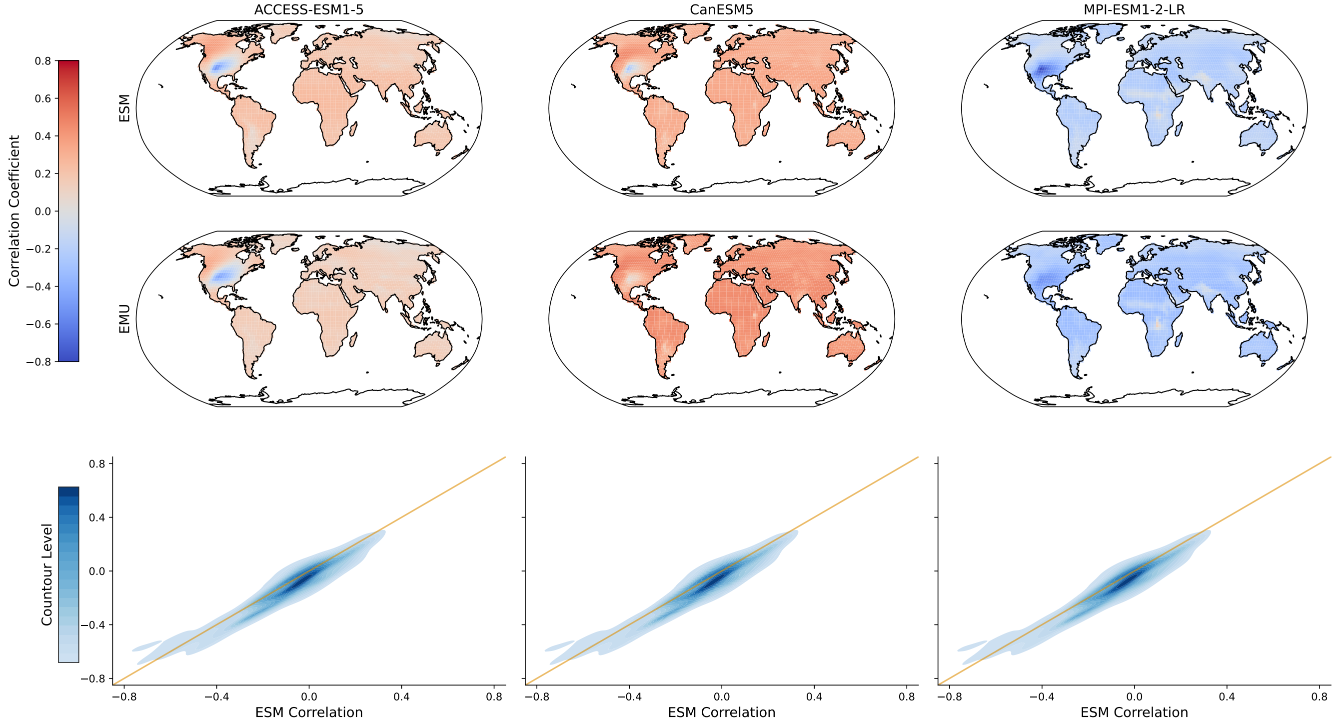

Figure C13. Same as Fig. 7 but for the coupled emulations in July.

https://doi.org/10.5194/egusphere-2024-278
Preprint. Discussion started: 13 May 2024
© Author(s) 2024. CC BY 4.0 License.

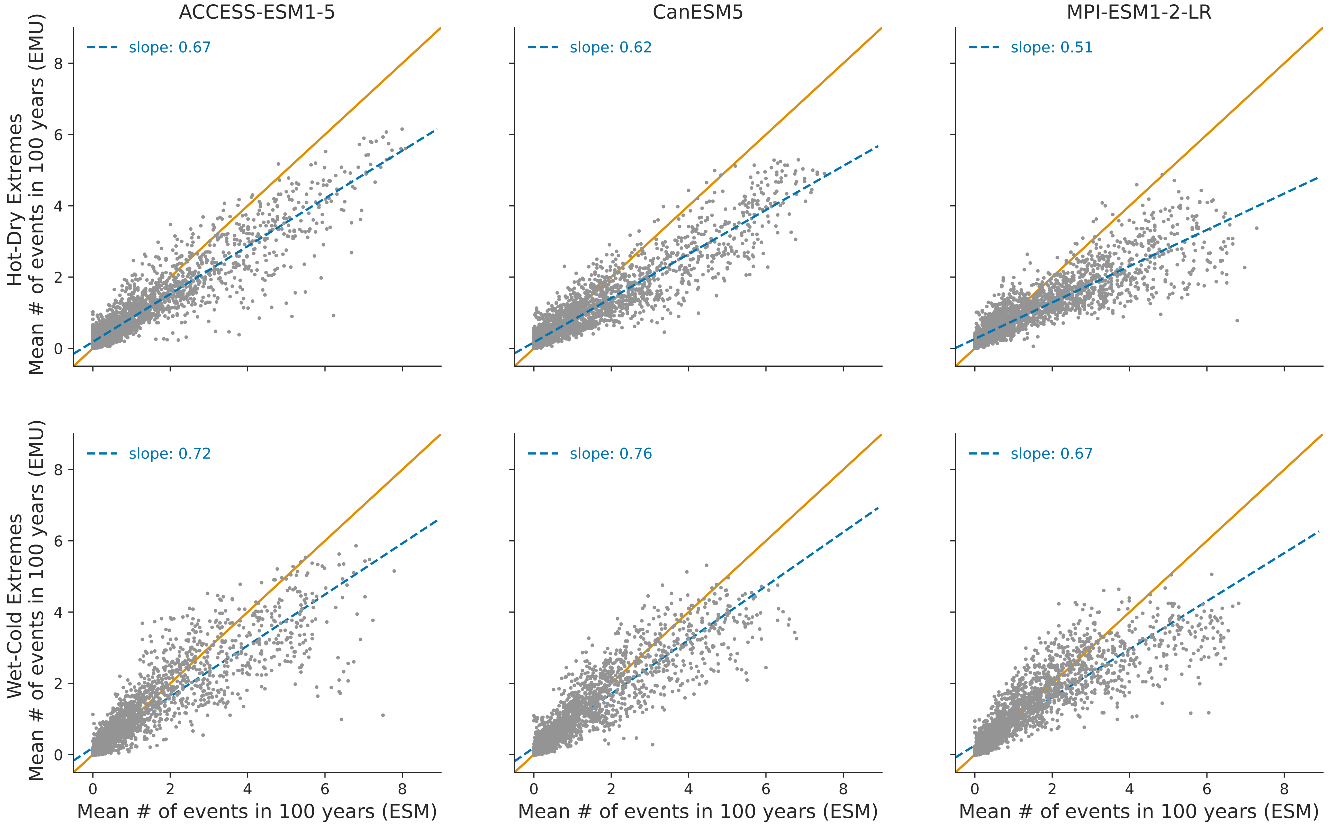

Figure C14. Same as Fig. 9 but for the coupled emulations in January.

https://doi.org/10.5194/egusphere-2024-278
Preprint. Discussion started: 13 May 2024
© Author(s) 2024. CC BY 4.0 License.

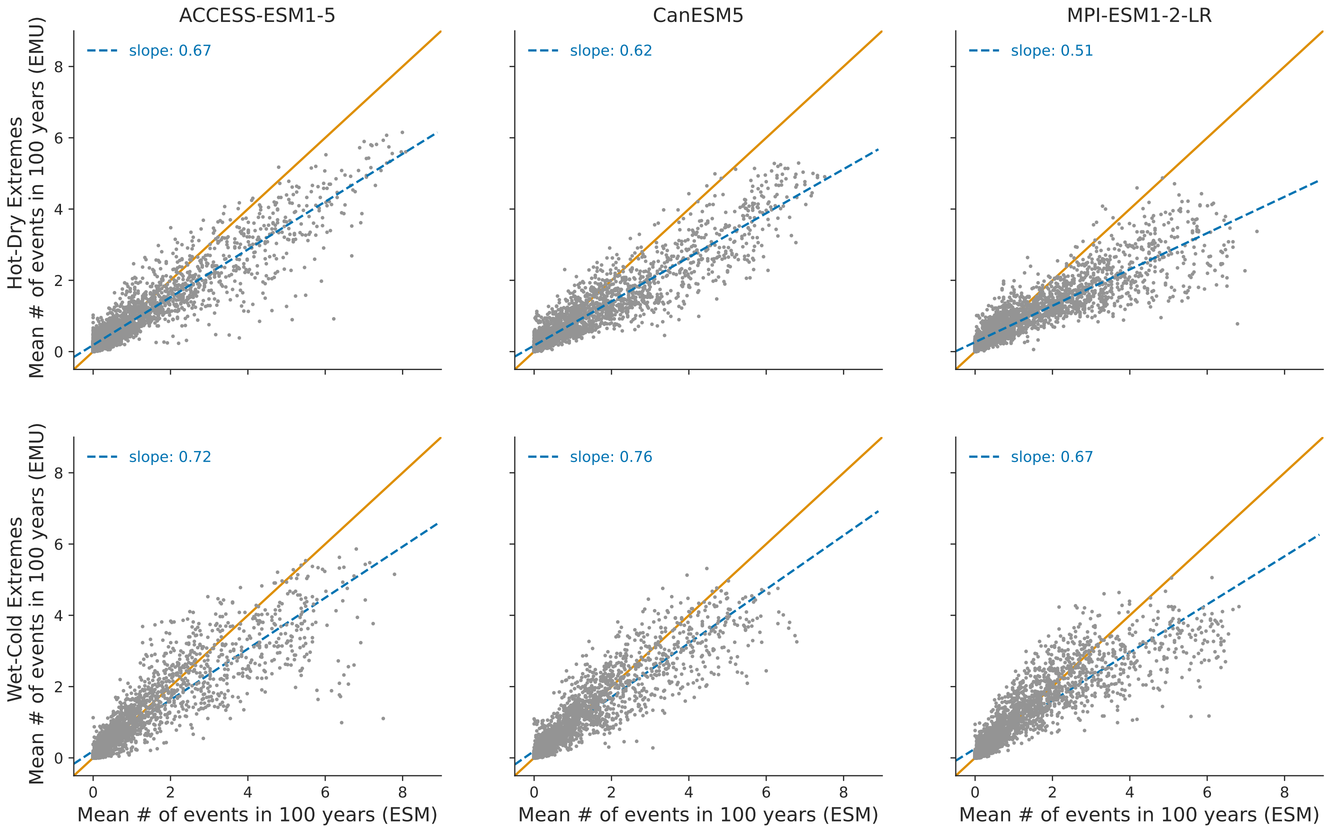

Figure C15. Same as Fig. 9 but for the coupled emulations in July.

Author contributions. S.S., L.G., S.I.S. and C.F.S. conceived the study. S.S. developed the methods with contributions from L.G. and P.P. S.S. wrote the manuscript with contributions from all authors.

420 *Competing interests.* The authors declare no competing interests.

Acknowledgements. S.S. acknowledges support by the German Federal Environmental Foundation (DBU). S.S., L.G., Q.L., P.P., S.I.S. and C.F.S. acknowledge funds by European Union's Horizon 2020 Research and Innovation Programme under Grant No. 101003687 (PROVIDE). L.G., M.H., and S.I.S. also acknowledge funds from the European Union's Horizon Europe research and innovation program under Grant No. 101081369 (SPARCCLE).

© Author(s) 2024. CC BY 4.0 License.

References

Abramoff, R. Z., Ciais, P., Zhu, P., Hasegawa, T., Wakatsuki, H., and Makowski, D.: Adaptation strategies strongly reduce the future impacts of climate change on crop yields, Authorea Preprints, 2022.

Allen, M. R. and Ingram, W. J.: Constraints on future changes in climate and the hydrologic cycle, Nature, 419, 224–232, 2002.

Bader, D. C., Leung, R., Taylor, M., and McCoy, R. B.: E3SM-Project E3SM1.1 model output prepared for CMIP6 ScenarioMIP, https://doi.org/10.22033/ESGF/CMIP6.15103, 2020.

Balaji, V., Maisonnave, E., Zadeh, N., Lawrence, B. N., Biercamp, J., Fladrich, U., Aloisio, G., Benson, R., Caubel, A., Durachta, J., Foujols, M.-A., Lister, G., Mocavero, S., Underwood, S., and Wright, G.: CPMIP: measurements of real computational performance of Earth system models in CMIP6, Geoscientific Model Development, 10, 19–34, https://doi.org/10.5194/gmd-10-19-2017, 2017.

Bentsen, M., Oliviè, D. J. L., Seland, y., Toniazzo, T., Gjermundsen, A., Graff, L. S., Debernard, J. B., Gupta, A. K., He, Y., Kirkevåg, A., Schwinger, J., Tjiputra, J., Aas, K. S., Bethke, I., Fan, Y., Griesfeller, J., Grini, A., Guo, C., Ilicak, M., Karset, I. H. H., Landgren, O. A., Liakka, J., Moseid, K. O., Nummelin, A., Spensberger, C., Tang, H., Zhang, Z., Heinze, C., Iversen, T., and Schulz, M.: NCC NorESM2-MM model output prepared for CMIP6 ScenarioMIP, https://doi.org/10.22033/ESGF/CMIP6.608, 2019.

Beusch, L., Gudmundsson, L., and Seneviratne, S. I.: Emulating Earth system model temperatures with MESMER: from global mean temperature trajectories to grid-point-level realizations on land, Earth System Dynamics, 11, 139–159, https://doi.org/10.5194/esd-11-139-2020, 2020.

Beusch, L., Nicholls, Z., Gudmundsson, L., Hauser, M., Meinshausen, M., and Seneviratne, S. I.: From emission scenarios to spatially resolved projections with a chain of computationally efficient emulators: coupling of MAGICC (v7.5.1) and MESMER (v0.8.3), Geoscientific Model Development, 15, 2085–2103, https://doi.org/10.5194/gmd-15-2085-2022, 2022.

Boucher, O., Denvil, S., Levavasseur, G., Cozic, A., Caubel, A., Foujols, M.-A., Meurdesoif, Y., Cadule, P., Devilliers, M., Dupont, E., and Lurton, T.: IPSL IPSL-CM6A-LR model output prepared for CMIP6 ScenarioMIP, https://doi.org/10.22033/ESGF/CMIP6.1532, 2019.

Brunner, L., Hauser, M., Lorenz, R., and Beyerle, U.: The ETH Zurich CMIP6 next generation archive: technical documentation, https://doi.org/10.5281/zenodo.3734128, 2020.

Cao, J.: NUIST NESMv3 model output prepared for CMIP6 ScenarioMIP, https://doi.org/10.22033/ESGF/CMIP6.2027, 2019.

Chandler, R. E.: Multisite, multivariate weather generation based on generalised linear models, Environmental Modelling & Software, 134, 104 867, 2020.

Danabasoglu, G.: NCAR CESM2 model output prepared for CMIP6 ScenarioMIP, https://doi.org/10.22033/ESGF/CMIP6.2201, 2019a.

Danabasoglu, G.: NCAR CESM2-WACCM model output prepared for CMIP6 ScenarioMIP, https://doi.org/10.22033/ESGF/CMIP6.10026, 2019b.

Dix, M., Bi, D., Dobrohotoff, P., Fiedler, R., Harman, I., Law, R., Mackallah, C., Marsland, S., O'Farrell, S., Rashid, H., Srbinovsky, J., Sullivan, A., Trenham, C., Vohralik, P., Watterson, I., Williams, G., Woodhouse, M., Bodman, R., Dias, F. B., Domingues, C. M., Hannah, N., Heerdegen, A., Savita, A., Wales, S., Allen, C., Druken, K., Evans, B., Richards, C., Ridzwan, S. M., Roberts, D., Smillie, J., Snow, K., Ward, M., and Yang, R.: CSIRO-ARCCSS ACCESS-CM2 model output prepared for CMIP6 ScenarioMIP, https://doi.org/10.22033/ESGF/CMIP6.2285, 2019.

Dobson, A. J. and Barnett, A. G.: An introduction to generalized linear models, CRC press, 2018.

Edwards, M., Castruccio, S., and Hammerling, D.: A Multivariate Global Spatiotemporal Stochastic Generator for Climate Ensembles, Journal of Agricultural, Biological and Environmental Statistics, 24, 464–483, https://doi.org/10.1007/s13253-019-00352-8, 2019.

Eyring, V., Bony, S., Meehl, G. A., Senior, C. A., Stevens, B., Stouffer, R. J., and Taylor, K. E.: Overview of the Coupled Model Intercomparison Project Phase 6 (CMIP6) experimental design and organization, Geoscientific Model Development, 9, 1937–1958, 2016.

George, J., Letha, J., and Jairaj, P.: Daily rainfall prediction using generalized linear bivariate model–a case study, Procedia Technology, 24, 31–38, 2016.

Good, P.: MOHC HadGEM3-GC31-LL model output prepared for CMIP6 ScenarioMIP, https://doi.org/10.22033/ESGF/CMIP6.10845, 2019.

Good, P., Sellar, A., Tang, Y., Rumbold, S., Ellis, R., Kelley, D., Kuhlbrodt, T., and Walton, J.: MOHC UKESM1.0-LL model output prepared for CMIP6 ScenarioMIP, https://doi.org/10.22033/ESGF/CMIP6.1567, 2019.

Gudmundsson, L. and Seneviratne, S. I.: Anthropogenic climate change affects meteorological drought risk in Europe, Environmental Research Letters, 11, 044 005, 2016.

Hauser, M., Gudmundsson, L., Orth, R., Jézéquel, A., Haustein, K., Vautard, R., Van Oldenborgh, G. J., Wilcox, L., and Seneviratne, S. I.: Methods and model dependency of extreme event attribution: the 2015 European drought, Earth's Future, 5, 1034–1043, 2017.

Hauser, M., Beusch, L., Nicholls, Z., Nath, S., Schwaab, J., and Quilcaille, Y.: ESMER-group/mesmer: version 0.9.0 (v0.9.0), Zenodo [code], https://doi.org/10.5281/zenodo.10408206, 2023.

Herger, N., Sanderson, B. M., and Knutti, R.: Improved pattern scaling approaches for the use in climate impact studies, Geophysical Research Letters, 42, 3486–3494, 2015.

Iturbide, M., Gutiérrez, J. M., Alves, L. M., Bedia, J., Cimadevilla, E., Cofiño, A. S., Cerezo-Mota, R., Di Luca, A., Faria, S. H., Gorodetskaya, I., et al.: An update of IPCC climate reference regions for subcontinental analysis of climate model data: definition and aggregated datasets, Earth System Science Data Discussions, 2020, 1–16, 2020.

Jackson, L.: MOHC HadGEM3-GC31-MM model output prepared for CMIP6 ScenarioMIP, https://doi.org/10.22033/ESGF/CMIP6.10846, 2020.

Jha, S., Gudmundsson, L., and Seneviratne, S. I.: Partitioning the uncertainties in compound hot and dry precipitation, soil moisture, and runoff extremes projections in CMIP6, Earth's Future, 11, e2022EF003 315, 2023.

Khouakhi, A., Villarini, G., and Vecchi, G. A.: Contribution of tropical cyclones to rainfall at the global scale, Journal of Climate, 30, 359–372, 2017.

King, A. D., Borowiak, A. R., Brown, J. R., Frame, D. J., Harrington, L. J., Min, S.-K., Pendergrass, A., Rugenstein, M., Sniderman, J. K., and Stone, D. A.: Transient and quasi-equilibrium climate states at 1.5 C and 2 C global warming, Earth's Future, 9, e2021EF002 274, 2021.

Lange, S.: Trend-preserving bias adjustment and statistical downscaling with ISIMIP3BASD (v1.0), Geoscientific Model Development, 12, 3055–3070, https://doi.org/10.5194/gmd-12-3055-2019, 2019.

Lehner, F., Deser, C., Maher, N., Marotzke, J., Fischer, E. M., Brunner, L., Knutti, R., and Hawkins, E.: Partitioning climate projection uncertainty with multiple large ensembles and CMIP5/6, Earth System Dynamics, 11, 491–508, 2020.

Li, L.: CAS FGOALS-g3 model output prepared for CMIP6 ScenarioMIP, https://doi.org/10.22033/ESGF/CMIP6.2056, 2019.

Link, R., Snyder, A., Lynch, C., Hartin, C., Kravitz, B., and Bond-Lamberty, B.: Fldgen v1.0: an emulator with internal variability and space–time correlation for Earth system models, Geoscientific Model Development, 12, 1477–1489, https://doi.org/10.5194/gmd-12-1477-2019, 2019.

Liu, G., Peng, S., Huntingford, C., and Xi, Y.: A new precipitation emulator (PREMU v1. 0) for lower-complexity models, Geoscientific Model Development, 16, 1277–1296, 2023.

Lovato, T. and Peano, D.: CMCC CMCC-CM2-SR5 model output prepared for CMIP6 ScenarioMIP, https://doi.org/10.22033/ESGF/CMIP6.1365, 2020.

Maher, N., Milinski, S., and Ludwig, R.: Large ensemble climate model simulations: introduction, overview, and future prospects for utilising multiple types of large ensemble, Earth System Dynamics, 12, 401–418, https://doi.org/10.5194/esd-12-401-2021, 2021.

McCullagh, P.: Generalized linear models, Routledge, 2019.

Nath, S., Lejeune, Q., Beusch, L., Seneviratne, S. I., and Schleussner, C.-F.: MESMER-M: an Earth system model emulator for spatially resolved monthly temperature, Earth System Dynamics, 13, 851–877, https://doi.org/10.5194/esd-13-851-2022, 2022.

Nychka, D., Hammerling, D., Krock, M., and Wiens, A.: Modeling and emulation of nonstationary Gaussian fields, Spatial statistics, 28, 21–38, 2018.

O'Neill, B. C., Tebaldi, C., Van Vuuren, D. P., Eyring, V., Friedlingstein, P., Hurtt, G., Knutti, R., Kriegler, E., Lamarque, J.-F., Lowe, J., et al.: The scenario model intercomparison project (ScenarioMIP) for CMIP6, Geoscientific Model Development, 9, 3461–3482, 2016.

Pfleiderer, P., Schleussner, C.-F., and Sillmann, J.: Limited reversal of regional climate signals in overshoot scenarios, Environmental Research: Climate, 2023.

Quilcaille, Y., Gudmundsson, L., Beusch, L., Hauser, M., and Seneviratne, S. I.: Showcasing MESMER-X: Spatially Resolved Emulation of Annual Maximum Temperatures of Earth System Models, Geophysical Research Letters, 49, e2022GL099 012, 2022.

Quilcaille, Y., Gudmundsson, L., and Seneviratne, S. I.: Extending MESMER-X: A spatially resolved Earth system model emulator for fire weather and soil moisture, EGUsphere, 2023, 1–35, 2023.

Schneider, T., Lan, S., Stuart, A., and Teixeira, J.: Earth system modeling 2.0: A blueprint for models that learn from observations and targeted high-resolution simulations, Geophysical Research Letters, 44, 12–396, 2017.

Schöongart, S.: MESMER-M-TP version 0.1.0, Zenodo [code], https://doi.org/10.5281/zenodo.11086167, 2024.

Schupfner, M., Wieners, K.-H., Wachsmann, F., Steger, C., Bittner, M., Jungclaus, J., Früh, B., Pankatz, K., Giorgetta, M., Reick, C., Legutke, S., Esch, M., Gayler, V., Haak, H., de Vrese, P., Raddatz, T., Mauritsen, T., von Storch, J.-S., Behrens, J., Brovkin, V., Claussen, M., Crueger, T., Fast, I., Fiedler, S., Hagemann, S., Hohenegger, C., Jahns, T., Kloster, S., Kinne, S., Lasslop, G., Kornblueh, L., Marotzke, J., Matei, D., Meraner, K., Mikolajewicz, U., Modali, K., Müller, W., Nabel, J., Notz, D., Peters-von Gehlen, K., Pincus, R., Pohlmann, H., Pongratz, J., Rast, S., Schmidt, H., Schnur, R., Schulzweida, U., Six, K., Stevens, B., Voigt, A., and Roeckner, E.: DKRZ MPI-ESM1.2-HR model output prepared for CMIP6 ScenarioMIP, https://doi.org/10.22033/ESGF/CMIP6.2450, 2019.

Schupfner, M., Wieners, K.-H., Wachsmann, F., Milinski, S., Steger, C., Bittner, M., Jungclaus, J., Früh, B., Pankatz, K., Giorgetta, M., Reick, C., Legutke, S., Esch, M., Gayler, V., Haak, H., de Vrese, P., Raddatz, T., Mauritsen, T., von Storch, J.-S., Behrens, J., Brovkin, V., Claussen, M., Crueger, T., Fast, I., Fiedler, S., Hagemann, S., Hohenegger, C., Jahns, T., Kloster, S., Kinne, S., Lasslop, G., Kornblueh, L., Marotzke, J., Matei, D., Meraner, K., Mikolajewicz, U., Modali, K., Müller, W., Nabel, J., Notz, D., Peters-von Gehlen, K., Pincus, R., Pohlmann, H., Pongratz, J., Rast, S., Schmidt, H., Schnur, R., Schulzweida, U., Six, K., Stevens, B., Voigt, A., and Roeckner, E.: DKRZ MPI-ESM1.2-LR model output prepared for CMIP6 ScenarioMIP, https://doi.org/10.22033/ESGF/CMIP6.15349, 2021.

Seferian, R.: CNRM-CERFACS CNRM-ESM2-1 model output prepared for CMIP6 ScenarioMIP, https://doi.org/10.22033/ESGF/CMIP6.1395, 2019.

Seland, y., Bentsen, M., Olivië, D. J. L., Toniazzo, T., Gjermundsen, A., Graff, L. S., Debernard, J. B., Gupta, A. K., He, Y., Kirkevåg, A., Schwinger, J., Tjiputra, J., Aas, K. S., Bethke, I., Fan, Y., Griesfeller, J., Grini, A., Guo, C., Ilicak, M., Karset, I. H. H., Landgren, O. A., Liakka, J., Moseid, K. O., Nummelin, A., Spensberger, C., Tang, H., Zhang, Z., Heinze, C., Iversen, T., and Schulz, M.: NCC NorESM2-LM model output prepared for CMIP6 ScenarioMIP, https://doi.org/10.22033/ESGF/CMIP6.604, 2019.

https://doi.org/10.5194/egusphere-2024-278
Preprint. Discussion started: 13 May 2024
© Author(s) 2024. CC BY 4.0 License.

Semmler, T., Danilov, S., Rackow, T., Sidorenko, D., Barbi, D., Hegewald, J., Pradhan, H. K., Sein, D., Wang, Q., and Jung, T.: AWI AWI-CM1.1MR model output prepared for CMIP6 ScenarioMIP, https://doi.org/10.22033/ESGF/CMIP6.376, 2019.

Seneviratne, S. I., Nicholls, N., Easterling, D., Goodess, C. M., Kanae, S., Kossin, J., Luo, Y., Marengo, J., McInnes, K., Rahimi, M., and et al.: Changes in Climate Extremes and their Impacts on the Natural Physical Environment, p. 109–230, Cambridge University Press, https://doi.org/10.1017/CBO9781139177245.006, 2012.

Snyder, A., Link, R., Dorheim, K., Kravitz, B., Bond-Lamberty, B., and Hartin, C.: Joint emulation of Earth System Model temperature-precipitation realizations with internal variability and space-time and cross-variable correlation: fldgen v2. 0 software description, Plos one, 14, e0223 542, 2019.

Song, Z., Qiao, F., Bao, Y., Shu, Q., Song, Y., and Yang, X.: FIO-QLNM FIO-ESM2.0 model output prepared for CMIP6 ScenarioMIP, https://doi.org/10.22033/ESGF/CMIP6.9051, 2019.

Swart, N. C., Cole, J. N., Kharin, V. V., Lazare, M., Scinocca, J. F., Gillett, N. P., Anstey, J., Arora, V., Christian, J. R., Jiao, Y., Lee, W. G., Majaess, F., Saenko, O. A., Seiler, C., Seinen, C., Shao, A., Solheim, L., von Salzen, K., Yang, D., Winter, B., and Sigmond, M.: CCCma CanESM5 model output prepared for CMIP6 ScenarioMIP, https://doi.org/10.22033/ESGF/CMIP6.1317, 2019.

Tabari, H.: Climate change impact on flood and extreme precipitation increases with water availability, Scientific reports, 10, 13 768, 2020.

Tebaldi, C. and Arblaster, J. M.: Pattern scaling: Its strengths and limitations, and an update on the latest model simulations, Climatic Change, 122, 459–471, 2014.

Tebaldi, C., Snyder, A., and Dorheim, K.: STITCHES: creating new scenarios of climate model output by stitching together pieces of existing simulations, Earth System Dynamics, 13, 1557–1609, https://doi.org/10.5194/esd-13-1557-2022, 2022.

Trenberth, K. E., Dai, A., Rasmussen, R. M., and Parsons, D. B.: The changing character of precipitation, Bulletin of the American Meteorological Society, 84, 1205–1218, 2003.

Voldoire, A.: CNRM-CERFACS CNRM-CM6-1 model output prepared for CMIP6 ScenarioMIP, https://doi.org/10.22033/ESGF/CMIP6.1384, 2019a.

Voldoire, A.: CNRM-CERFACS CNRM-CM6-1-HR model output prepared for CMIP6 ScenarioMIP, https://doi.org/10.22033/ESGF/CMIP6.1388, 2019b.

YU, Y.: CAS FGOALS-f3-L model output prepared for CMIP6 ScenarioMIP, https://doi.org/10.22033/ESGF/CMIP6.2046, 2019.

Yukimoto, S., Koshiro, T., Kawai, H., Oshima, N., Yoshida, K., Urakawa, S., Tsujino, H., Deushi, M., Tanaka, T., Hosaka, M., Yoshimura, H., Shindo, E., Mizuta, R., Ishii, M., Obata, A., and Adachi, Y.: MRI MRI-ESM2.0 model output prepared for CMIP6 ScenarioMIP, https://doi.org/10.22033/ESGF/CMIP6.638, 2019.

Ziehn, T., Chamberlain, M., Lenton, A., Law, R., Bodman, R., Dix, M., Wang, Y., Dobrohotoff, P., Srbinovsky, J., Stevens, L., Vohralik, P., Mackallah, C., Sullivan, A., O'Farrell, S., and Druken, K.: CSIRO ACCESS-ESM1.5 model output prepared for CMIP6 ScenarioMIP, https://doi.org/10.22033/ESGF/CMIP6.2291, 2019.